INVITED PAPER

Structured Semiconductor Interfaces: Active Functionality on Light Manipulation

This article presents tunable and reconfigurable metasurfaces based on semiconductor nanoparticles, discussing their potential impact in interface-based nanophotonics.

By Yao-Wei Huang, He-Xiu Xu, *Senior Member IEEE*, Shang Sun, Yunkai Wu, Zhuo Wang, Shumin Xiao, Wei Xiang Jiang, *Member IEEE*, Tie Jun Cui, *Fellow IEEE*, Din Ping Tsai, *Fellow IEEE*, and Cheng-Wei Qiu, *Member IEEE*

Manuscript received February 10, 2019; revised May 18, 2019; accepted May 19, 2019. Date of publication June 18, 2019; date of current version April 28, 2020. The work of Y.-W. Huang was supported by the National Research Foundation, Prime Minister's Office, Singapore, through the Competitive Research Program (CRP), under Award NRF-CRP15-2015-03. The work of H.-X. Xu was supported in part by the Key Program of the Natural Science Foundation of Shaanxi Province under Grant 2017KJXX-24, in part by the China Association for Science and Technology under Grant 17-JCJQ-QT-003, and in part by the Aviation Science Foundation of China under Grant 20161996009. The work of Z. Wang was supported by the National Natural Science Foundation of China under Grant 61805159. The work of W. X. Jiang was supported by the Foundation of National Excellent Doctoral Dissertation of China under Grant 201444 and in part by the National Ten-Thousands Telents Plan. The work of T. J. Cui was supported by the National Key Research and Development Program of China under Grant 2017YFA0700201, Grant 2017YFA0700202, and Grant 2017YFA0700203. The work of D. P. Tsai was supported in part by the Ministry of Science and Technology, Taiwan, under Grant MOST-107-2112-M-001-042-MY3, in part by Academia Sinica under Grant AS-TP-108-M12, and in part by the National Center for Research Center for Applied Sciences. The work of C.-W. Qiu was supported in part by the National Research Foundation, Prime Minister's Office, Singapore, through the Competitive Research Program (CRP), under Award NRF-CRP15-2015-03, and in part by the A*STAR Pharos Program under Project R-263-000-B91-305 and Grant 152 70 00014. (*Yao-Wei Huang, He-Xiu Xu, and Shang Sun contributed equally to this work.*) (*Corresponding authors: Yao-Wei Huang; Cheng-Wei Qiu.*)

Y.-W. Huang, **S. Sun**, and **C.-W. Qiu** are with the Department of Electrical and Computer Engineering, National University of Singapore, Singapore 117583 (e-mail: elehyw@nus.edu.sg; eleqc@nus.edu.sg).

H.-X. Xu is with the Air and Missile Defense College, Air Force Engineering University, Xi'an 710051, China.

Y. Wu and **S. Xiao** are with the State Key Laboratory on Tunable Laser Technology, Ministry of Industry and Information Technology Key Lab of Micro-Nano Optoelectronic Information System, Shenzhen Graduate School, Harbin Institute of Technology, Shenzhen 518055, China.

Z. Wang is with the International Collaborative Laboratory of 2D Materials for Optoelectronics Science and Technology, Shenzhen University, Shenzhen 518060, China.

W. X. Jiang and **T. J. Cui** are with the State Key Laboratory of Millimeter Waves, Southeast University, Nanjing 210096, China.

D. P. Tsai is with the Research Center for Applied Sciences, Academia Sinica, Taipei 11529, Taiwan, with the Department of Physics, National Taiwan University, Taipei 10617, Taiwan, and also with the Department of Material Science and Engineering, National Tsing Hua University, Hsinchu 300, Taiwan.

Digital Object Identifier 10.1109/JPROC.2019.2919675

ABSTRACT | Structured interfaces with subwavelength features enable modulations of phase, amplitude, and polarization on demand, leading to a plethora of flat-profile devices and metasurfaces. Plasmonic and dielectric metasurfaces have been intensively explored, building up the frameworks of flat optics for ultrathin and integrated nanophotonics. The *in situ* controllability and tunability of aforementioned family of metasurfaces, however, has been a grand challenge, due to the intrinsic limitations of the materials. Semiconductors with diversified catalogs of material candidates thus demonstrate promising potentials, owing to the mature and versatile technologies developed nowadays. The fuse of semiconductors and nanostructured metasurfaces has been witnessed more recently, paving a distinct avenue toward active, tunable, reconfigurable light manipulation for next-generation optical nanodevices. Judicious selection of the active materials for metasurfaces empowers the active functionality of the designer applications. This paper presents a review of this merging semiconductor paradigm for active metasurfaces across a wide range of spectrum and shows unprecedented potentials in the future interface-based optoelectronics, quantum optics, nano-optics, and surface engineering with full compatibility of semiconductor foundry.

KEYWORDS | Active materials; active tuning; metasurfaces; phase engineering; semiconductors.

I. INTRODUCTION

Metasurfaces are flat interfaces composed of subwavelength artificial media (metaatoms) showing tailored properties of electromagnetic (EM) wave on demand [1]–[4].

By controlling the phase delay and/or amplitude by each of the metaatoms, one can realize metasurfaces that would enable complex wavefront engineering and the development of a generalized form of Snell's law [5]. The flat optics open new pathways to realize flat lens [6], [7], holography [8], and optical vortex generation [9], among others. Due to the flat-profile nature of metasurfaces, it even demonstrates some potentials in replacing the bulky 3-D optical elements in the optical systems, such as biomedical endoscopic imaging [10], computational imaging [11], and augmented reality (AR) [12], [13]. However, passive element-based metasurfaces present a static feature once they are fabricated. Dynamic control of metasurfaces with postfabrication modulation to achieve arbitrary control of phase, amplitude, and/or polarization of individual metaatoms is the holy grails in this field.

Various tuning mechanisms have been studied and reported, such as electrooptic modulation [14], magnetoelastic control [15], mechanical stretching [16], [17], micro-nanoelectromechanical systems (M-NEMS) [18], and thermo-optic modulation [19]. There are many review articles about tunable and reconfigurable metasurfaces [20], active material-based metasurfaces [21], and light-induced tunable metasurfaces [22]. However, most of the reviews focus on the classifications of the functionalities and/or performance control methods, such as by switching spin, polarization, and wavelengths of the input light. A comprehensive material-paradigm review to address the complementary nature between versatile new materials and advanced active metasurfaces is still missing. In particular, this era has been an era of materials, and metasurface area is not an exception either. In this paper, we focus on the hybrid metasurfaces with semiconductors as active materials and mainly discuss the electrical and optical tuning mechanisms. Since semiconductors show mature and versatile technologies and foundry-ready compatibility, we believe that the semiconductor-based metasurface will play a pivotal role in bridging the gaps between fundamental science, industrial adoption, and mass production.

In Sections II–VI, we overview the recent developments of functions and applications in metasurfaces hybridized with or made of semiconductors. We categorize the sections with different catalogs of semiconductors, such as transparent conductive oxides (TCOs), 2-D materials, phase change materials (PCMs), silicon, and III–V semiconductors. The versatile modulation methods are also discussed, depending on the properties of the active materials, including electrical, optical, and thermal modulation. The various active functionalities, e.g.,phase, amplitude, and polarization modulation will also be discussed in each category, along with possible schemes to obtain faster, high-efficiency active metasurfaces.

II. TRANSPARENT CONDUCTIVE OXIDES

TCO is one typical kind of transparent heavily doped n-type semiconductors well applied in our daily electric appliances. The TCO materials, such as indium–tin oxide (ITO), doped zinc oxide (e.g., Al:ZnO and Ga:ZnO), and doped cadmium oxide (e.g., CdO:In), have much lower loss than that of gold and silver in the visible and near-infrared (NIR) region [23]–[25]. The dielectric permittivity of TCOs can be described by the Drude model where the plasma frequency is related to the carrier density. One can modulate the permittivity of TCOs by controlling the doping concentration to achieve epsilon-near-zero (ENZ) at the desired wavelength. TCOs can also be electrically tuned by applying static electric field (change of carrier density) and optically tuned (change of plasma frequency or plasma damping) due to its nonlinear properties.

A. Electrical Modulation

Metal–oxide–semiconductor (MOS) configuration is a common method to apply static electric field on TCOs [see Fig. 1(a), top] where TCOs are used as the active semiconductor layer [26]–[29]. When applied 0 or negative bias between metal and TCOs, the conduction band (E_c) and the valence band (E_v) of the active material at the surface are brought into a definite energy relationship with the Fermi level of metal. The band structure and carrier concentration follow the boundary conditions of the Poison equation and drift-diffusion equation. At thermal equilibrium, TCOs usually have a depletion layer around few-nanometer-thick near insulator, where the carrier concentration is lower than intrinsic doping [see Fig. 1(a), middle]. On the other hand, when applying sufficient positive bias, accumulation layer forms at the same position where the carrier concentration is higher than intrinsic doping [see Fig. 1(a), bottom]. The formed depletion or accumulation layer is the so-called field-effect modulation because of the large variation of electric field and the permittivity [26], [30]. This phenomenon has been used to demonstrate electrically controlled plasmonic waveguides [27], [30]–[32], metamaterials [33], [34], emission control [35], amplitude modulators [36], [37], and phase modulators [38]–[40].

Based on the field-effect modulation, top-gated [see Fig. 1(b) and (c)] [38], back-gated [see Fig. 1(d) and (e)] [39], and dual-gated metasurfaces [see Fig. 1(f) and (g)] [40] have been demonstrated in the NIR region. These metasurfaces provide both MOS configuration and plasmonic reflective metasurfaces (metalantenna/dielectric/metal-mirror) [41], [42], where the insulator and TCO layers are regarded as the dielectric layer. The operation wavelength of metasurfaces is controlled by the antenna geometry, while the phase can be electrically tuned by the dramatic change of plasmonic modes. By selecting specific doping of ITO, one can design a tunable metasurface that the active layer and the ENZ region form at the operation wavelength under reasonable bias applied. The top-gated metasurface has been demonstrated around 184° phase change with little amplitude change at 1550 nm [see Fig. 1(c)] and around

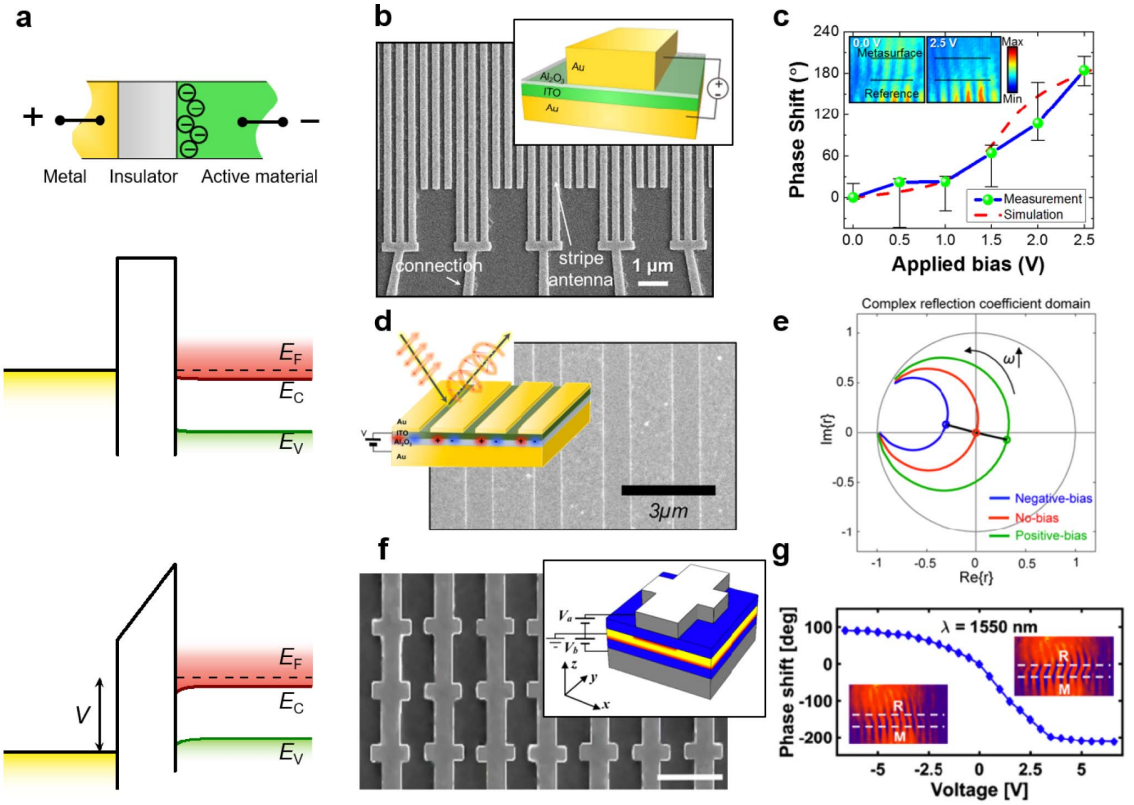

Fig. 1. ***Electrically tunable metasurfaces using TCO. (a) Schematic of the MOS field-effect dynamic (top) and its energy band diagram under applying 0 bias (middle) and V volt (bottom). (b) Top-gated ITO metasurfaces and (c) measured phase [38]. (d) Back-gated ITO metasurfaces and (e) its achievable complex reflection coefficient [39]. (f) Dual-gated metasurfaces and (g) measured phase [40]. Scale bar is 500 nm in (f).***

30% reflectance modulation ratio out of the operation wavelength under the applied bias of 2.5 V [38]. The modulation frequency can get higher than 2 MHz. The back-gated metasurfaces have been demonstrated a similar phase change at 5.94 μm via tuning the resonant scattering by changing the applied bias from -40 to $+40$ V [39]. The achievable complex reflection coefficient is shown in Fig. 1(e). The dual-gated metasurface incorporates two independent field-effect channels, resulting in a wider phase tunability [around 303° as shown in Fig. 1(g)] and a larger reflectance modulation ratio (around 89%) under the applied bias of 6.5 V [40].

B. Optical Modulation

In addition to electrical modulation, TCO properties can also be altered by optical excitation. The basic idea is that for a given change in the permittivity ($\Delta\varepsilon$), the resulting change in the refractive index (Δn) is given for a lossless material by $\Delta n = \Delta\varepsilon/(2\sqrt{\varepsilon})$. While the permittivity becomes small (e.g., in the ENZ region), the change of refractive index becomes large. Some studies have investigated the third- and second-harmonic generations in the ITO film [43], [44] and ultrafast optical switching (reflectance) in the AZO film [45]. The improvement of nonlinearity enhancement of ITO has been reported by exploiting hot electrons in ITO. The hot-electron injection from patterned plasmonic nanoantennas to ITO films under the excitation of femtosecond laser pulses results in ultrafast nonlinear control [46] and active control of plasmon-induced transparency [47], [48] and chirality [49]. ITO film itself can further achieve a refractive index change of 0.72 in the ITO's ENZ region [50]. The wavelength-dependent effective nonlinear refractive index coefficient n_2 with different angles of incidence is shown in Fig. 2(a). The measured value of $n_2 = 0.11$ cm^2/GW is around 1837 times larger than that at not-ENZ-region condition, while the effective nonlinear attenuation constant β is around 2377 times larger. The nonlinearity primarily results from the modification of the energy distribution of conduction-band electrons as a consequence of the laser-induced electron heating. Fig. 2(b) shows the free-electron temperature (T_e) changes with wavelength and angle of incidence. It goes higher, while the ENZ condition holds and free carrier absorption increases, resulting in an effective red shift in the material's plasma frequency and the change of permittivity $\Delta\varepsilon$ [50]. The plasma frequency of ITO is governed by the conduction-band nonparabolicity at higher electron temperature [see Fig. 2(c)] [51], [52], where the energy-wavevector dispersion relation for a

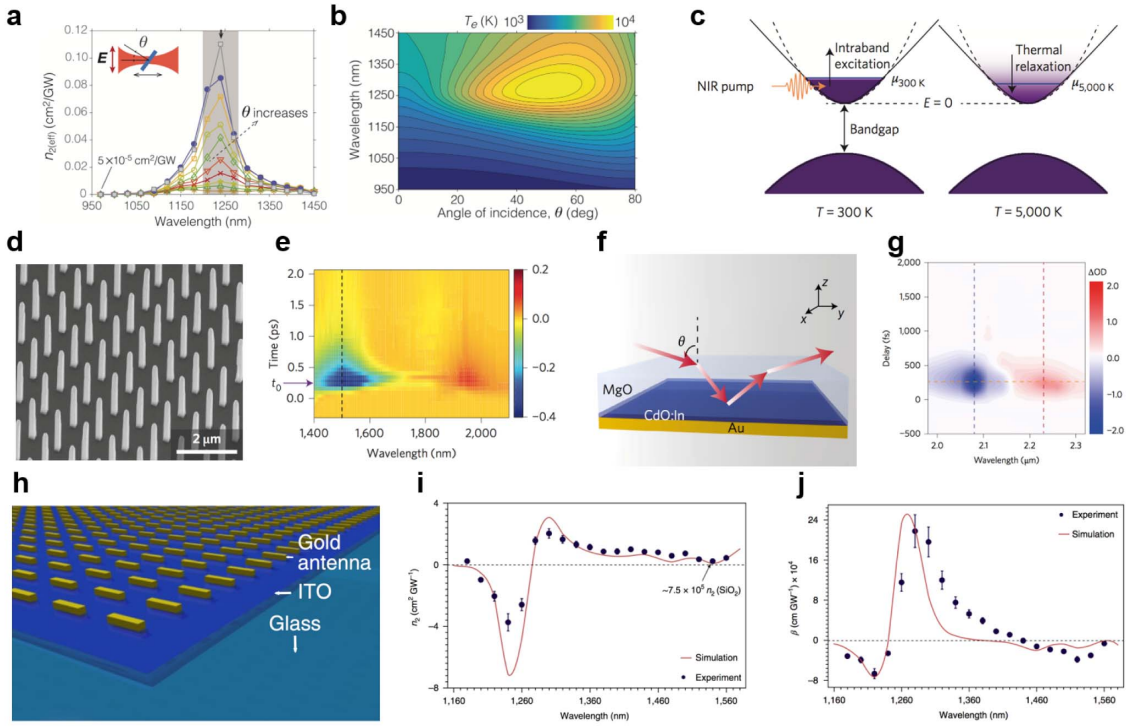

Fig. 2. ***Optical nonlinearity of TCOs. (a) Measured nonlinear effective refractive index and (b) calculated free-electron temperature of ITO film [50]. (c) Schematic showing the electron configurations and electronic processes involved in the NIR intraband pumping [52]. (d) ITO nanorod arrays and (e) Δ OD spectral map under a pump [52]. (f) Indium-doped cadmium oxide-based perfect absorber and (g) Δ OD spectral [55]. Gold nanoantennas coupled to (h) ITO for (i) large effective nonlinear refractive index and (j) nonlinear absorption [56].***

conduction-band electron follows Kane's model [53], [54]. An elevated electron temperature can also increase plasma damping [55]. The transient behavior of the localized surface plasmon resonances of patterned ITO, such as ITO nanorod array, achieves peak change in optical density ΔOD [defined as $\mathrm{t}\log10(T_{ON}/T_{OFF})$] of t0.37, giving an estimated 24% absolute transmission change [see Fig. 2(d) and (e)] [52]. A high-quality factor mode, such as Berreman-type perfect absorber using high-mobility indium-doped cadmium oxide (CdO), leads to a higher absolute change (in reflectance from 1.0% to 86.3%), resulting from the transient increase of the ensemble-averaged effective electron mass [see Fig. 2(f) and (g)] [55]. Furthermore, a large broadband nonlinear response is investigated from the ENZ-region of ITO coupled with gold antenna [see Fig. 2(h)], which achieves n_2 of t3.73 cm^2/GW with β of around 2.2 $\times$ 10^5 cm/GW [see Fig. 2(i) and (j)] [56]. Note that both n_2 and β can be positive or negative. The nonlinear response time of the TCOs is a few hundreds of femtoseconds [50], [52], [55], [56], which may enable applications in ultrafast lasing, optical limiters, and optical switching.

III. TWO-DIMENSIONAL MATERIALS

Benefitting from their electrical and optical properties, graphene and other 2-D materials, such as transition metal dichalcogenides (TMDs or TMDCs), black phosphorus (BP), and hexagonal boron nitride (hBN), have been widely studied and utilized in electrical and photonic devices these years [57]. The 2-D feature provides the possibilities for 2-D materials to be promising plasmonic materials in a wide spectral range covering from the infrared to terahertz regions [58], [59]. In contrast to the conventional plasmonic devices made of noble metals, plasmons in 2-D materials exhibit extremely tight field confinement and long propagation distance. Furthermore, the response is electrically and chemically tunable, which is an extraordinary feature for the investigation of the fundamental properties of plasmon itself and the potential applications. It is a novel platform for tunable devices, especially photonic metasurfaces [60]–[63]. hBN, with a large bandgap of around 6 eV, is an ideal 2-D dielectric material, which has not been deeply exploited in the field of active metasurfaces except some recent studies and applications on enhanced quantum emitters [64] and phonon polariton engineering [65], [66]. By virtue of few reports on metasurfaces integrated with hBN, in what follows, we focus on some typical 2-D materials (graphene, TMDs, and BP) to illustrate their fundamental properties, operation principle, and possible applications for metasurfaces.

A. Graphene Active Metasurfaces

Graphene, probably the best known 2-D material, consists of a single atomic layer of carbon in a hexagonal lattice. In its band structure, at the so-called Dirac points in

the first Brillouin zone, the conduction and valance bands touch each other. Close to the Dirac points, the electron energy follows a linear dispersion relationship, $E \approx \hbar v_F k$, where $v_F(\sim 10^6$ m/s) ($\sim 10^6$ m/s) is the Fermi velocity, which makes graphene semimetallic and leads to many exceptional electrical and optical properties. The Fermi energy is $E_F \approx \hbar v_F k_F$, where $k_F \approx \sqrt{\pi n}$ is the Fermi wave vector and n is the charge carrier concentration. Two kinds of transitions can be excited when photons are absorbed by graphene, which can be described by optical conductivity of graphene under random phase approximation (RPA) in the local limit [67], [68]. For undoped single-layer graphene ($n = 0$ and $E_F = 0$), its absorption exhibits frequency-independent properties, about 2.3% from visible to NIR spectral range. Once the graphene is electrically doped and charge carriers are injected, $2E_F$ bandgap opens and varies at applied bias voltage, making the optical absorption strongly dependent on the sheet carrier density. Considering the real situations based on electric gating, the Fermi energy can be boosted to 1 eV and the corresponding charge carrier concentration is at a value around 7×10^{13} cm^{-2} [69]. Thus, with attractive plasmonic properties, high carrier mobility, and electrostatic tunability, graphene can help manipulate EM waves at a deep-subwavelength scale and promise an avenue to active metamaterials [70].

Despite all the potentials, the interaction between continuous graphene and free space radiation is limited by low efficiency of plasmon excitations. To solve this problem, patterning graphene into subwavelength structures, such as microribbon arrays [see Fig. 3(a)], is a practical way. It offers an additional momentum and energy to match the properties of surface plasmons on the graphene film, giving rise to remarkable absorption peaks [71], [72]. Furthermore, closely packed nanodisks with electrostatic doping [73] and positioning doped graphene nanopatterns above a metallic reflector [74] can further enhance the absorption to 30% and 100%, respectively. Due to the electrical tunability of graphene, plasmonic resonances of graphene metasurfaces, such as nanodisk array as shown in Fig. 3(b) and (c), can exhibit broadband tunability [75]. As small as 15-nm-width graphene resonators can highly confine plasmonic modes with local density of optical states 10^6 larger than that in free space, which are supported and sensitive to the sheet charge density, making large frequency range tuning possible [76]. However, exciting plasmonic resonances in single-layer graphene resonators always requires high doping levels, which limits their applications. Using patterned multilayer graphene/insulator stacks instead of single-layer graphene is an effective way to realize higher carrier density and further enhance the plasmonic resonance frequency and magnitude. Furthermore, carriers are redistributed within different layers, making the plasmonic effects of electrostatic biasing enhanced and leading to broad spectral tuning range [77], [78]. Besides, patterned graphene is also utilized to realize large dynamic phase range and light manipulating, such as beam steering [79]–[81], focusing [82], cloaking [see Fig. 3(d)] [83], 84], and broadband absorber [85].

A lot of applications related to graphene active metasurfaces were demonstrated. With the help of interaction between standing plasmon excitations in arrays of graphene nanoribbons and surface polar phonons of the SiO_2 substrate, Freitag *et al.* [86] designed polarization-sensitive graphene photodetectors with narrow spectral-width resonances, allowing efficient tuning of modes by a gate voltage. Apart from photodetectors, Brar *et al.* [87] utilized graphene resonators to realize narrow spectral blackbody emission [see Fig. 3(e)]. In such design, when the patterned graphene sheets are heated, the pathways of infrared absorption and thermal emission are linked. The plasmonic resonant modes can therefore couple to free space and give rise to thermal emission with graphene sheets working as antennas. Based on gate tuning of the carrier density in graphene, both the intensity and the frequency can be electronically controlled [see Fig. 3(f)] [87]. Patterned graphene also offers great potentials for biosensing in the midinfrared range attributed to the ability of graphene plasmons for extremely field confinement, which helps enhance light–matter interactions. More importantly, by tuning the plasmonic resonances of graphene nanoribbons in mid-IR with gate bias voltage accordingly [see Fig. 3(g)], label-free probing of the proteins at different frequencies with high sensitivity can be realized [88].

Electrical connections are essential for gate-controlled graphene devices, which greatly restrict the flexibility of applications. Utilizing elastic vibration based on flexural waves to modulate graphene may be a genuine attempt. By varying the acoustic frequency that controls the effective grating period, the radiation pattern, beam angle, and frequency of operation can be dynamically tuned [89]. Ultraviolet illumination is another practical optional way to realize dynamically tuning of plasmonic resonances in graphene. As shown in Fig. 3(h), once the operational wavelength, power density, and illuminating duration time of UV light are properly set, Fermi level of graphene and corresponding response will be well modified accordingly [90].

B. Hybrid Graphene Active Metasurfaces

Despite that patterned graphene metasurfaces could exhibit tunability of EM resonances, the radiative coupling is still too weak. Strong light confinement of metallic plasmonic metasurfaces is widely used to promote the interactions between EM waves and matters around. Thus, by integrating graphene in the hot spots of conventional plasmonic metasurfaces and changing its carrier density, tunability of resonances can be greatly enhanced. Integrating split-ring resonators (SRRs) or dipole antennas on top of graphene have been employed to realize tunable intensity modulators with modulation depth from 11.5% [91]

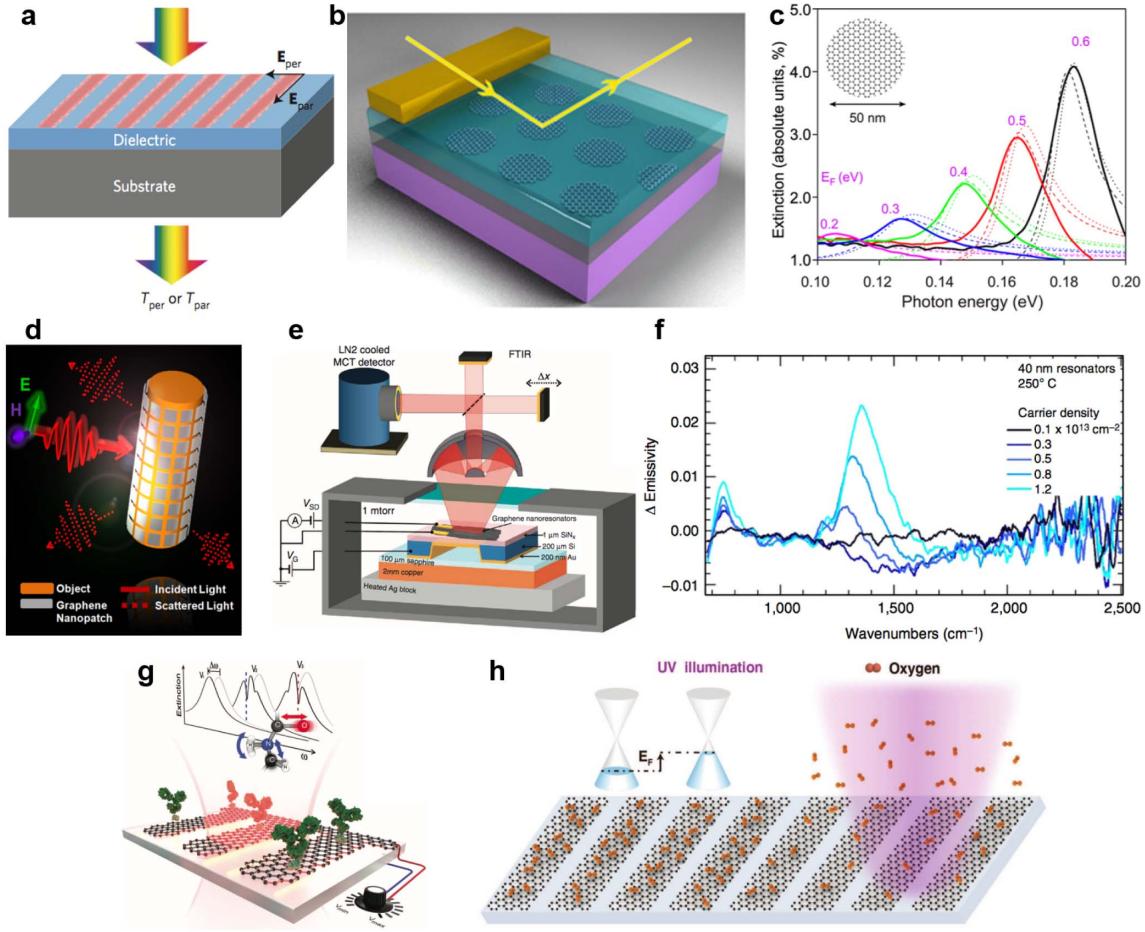

Fig. 3. ***Graphene active metasurfaces. (a) Midinfrared plasmons excitation for graphene nanoribbons [72]. (b) Graphene nanodisk array and (c) its extinction spectra under different applied voltages ΔV [75]. (d) THz cloaking device based on the graphene-nanopatch metasurface [83]. (e) Graphene plasmonic resonators and (f) tunable electronic control of blackbody emission [87]. (g) Tunable graphene mid-IR biosensor [88]. (h) Dynamical tuning of the Fermi level of graphene structure by using UV illuminations [90].***

to 30% [see Fig. 4(a)] [68]. Extraordinary optical transmission, always realized with subwavelength apertures in a metallic film, becomes an ideal scheme for transmission modulators. Owing to the ability of dense energy concentration, the large modulation depth of 50% in the terahertz frequency region was demonstrated [92]. It is essential to have a high Q-factor and narrow spectral width, e.g., Fano resonance, in order to reach a high modulation depth. High sensitivity and large field enhancement of hybrid metasurfaces composed with graphene and Fano antennas exhibit good performances for amplitude modulators [93], [94] and photodetectors [95]. Graphene hybridized with a periodic array of gold slits serves as a strategy to realize highly efficient modulators [96], [97], with modulation depth nearly 100% [shown in Fig. 4(b)]. In another work, a metal–insulator–metal waveguides metasurface on graphene with 20-nm gap size realized a broad resonance wavelength tuning range of 1100 nm at the midinfrared region [98]. By incorporating with a subwavelength-thick optical cavity, this structure furthermore behaves as an optical modulator over a broad wavelength range (5–7 μm) and perfect absorber with a modulation depth of up to 100% [99]. In addition to continuous graphene layers, graphene ribbons were also adopted and placed in the subwavelength gold slits. Plasmonic resonances of graphene ribbons work synergistically with plasmonic nanostructures as shown in Fig. 4(c), which give rise to more efficient modulations from 60% [100] to 100% [101], [102].

In addition to intensity modulations, phase modulations are investigated. In order to make metasurface response actively controllable, Lee *et al.*[103] made metaunits exhibiting Fano responses and continuous graphene layers configured together as shown in Fig. 4(d) and realized an electrically tunable extraordinary optical transmission modulation of terahertz waves with an amplitude of 47% and a phase of 32.2°. The phase modulation could be further improved to 55° by devising a Fano resonant plasmonic metasurface that contains nanoscale gaps with monolayer graphene [104]. Another tunable metasurface

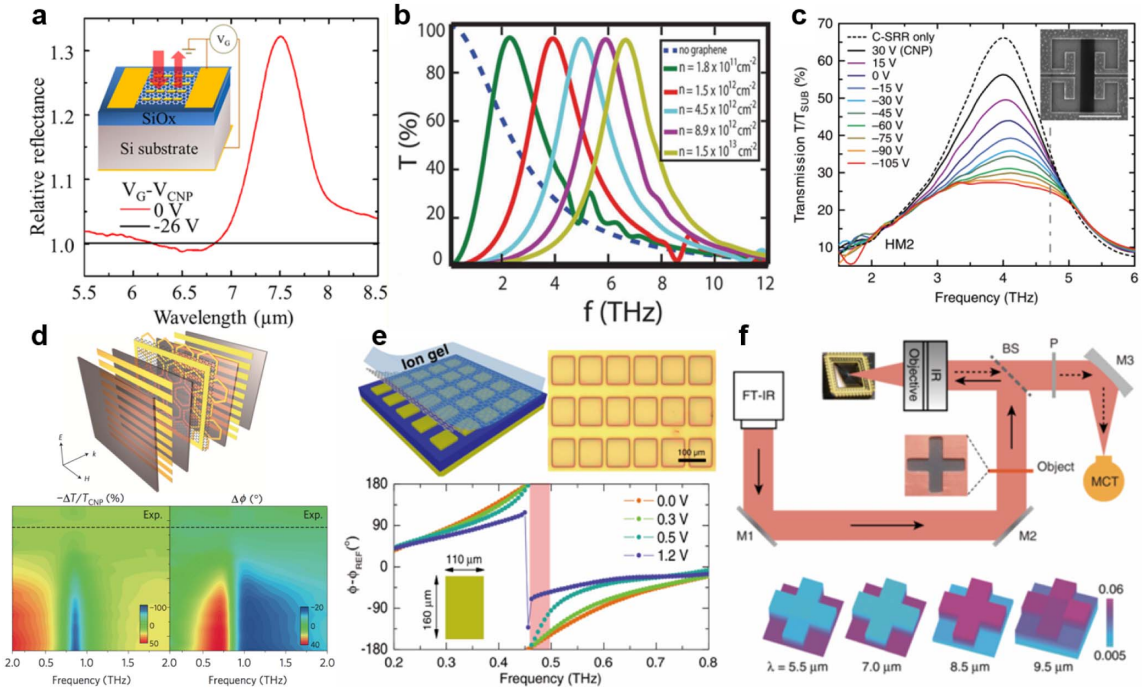

Fig. 4. ***Hybrid graphene active metasurfaces. (a) Tunable plasmonic device with antenna array on a gated graphene sheet and the relative reflectance spectrum indicating a maximum modulation depth of more than 30% [68]. (b) Transmission through the meta-graphene grating for different carrier density levels [97]. (c) Transmission spectra of the graphene ribbon hybrid metamaterial devices at different back-gate voltages [100]. (d) Schematic of gate-controlled terahertz active graphene metamaterial (top) and relative change in transmission (bottom left) and phase change (bottom right) plotted as a function of gate voltage based on the Fano responses [103]. (e) Schematic (top left) and an optical image (top right) of gate-controlled phase modulation with reflective hybrid graphene metasurface and the gate-dependent reflection phase spectra (bottom) [106]. (f) Schematic of the single-pixel imaging with hybrid graphene metasurface [112]. Scale bar is 1 μm in (c).***

design is based on gap-mode reflective metasurfaces (metal-antenna/dielectric/metal-mirror) [105]. A critical transition of phase will occur, leading to a phase modulation as large as around 240°, which can be used to realize reconfigurable metasurfaces such as tunable polarizer [see Fig 4(e)] [106] or beam-steering devices [107]. Recently, by incorporating graphene supercapacitor with split-ring resonators, a tunable metadevice was proposed. Phase modulation of 90° with amplitude modulation of 50 dB were experimentally demonstrated via electrically reconfigurable and spatially varying metaatoms [108]. Nowadays, many applications based on this configuration have been experimentally or numerically demonstrated, such as slow light devices [109], chiral metadevices [110], [111], spatial light modulator [see Fig. 4(f)] [112], dynamical vector vortex beam generator [113], and dual-band light focusing [114].

C. Transition Metal Dichalcogenides and Black Phosphorus

Unlike graphene, TMDs with bandgaps show great advantages such as low insertion loss and relatively large optical absorption, enhanced modulation depths, and strong near-field enhancement. Metasurfaces based on TMDs and BP have not been fully investigated. There have been several interesting applications proposed recently. Integrated MoS_2 and WSe_2 as active layers with plasmonic metamaterials and THz modulators are demonstrated [115], [116]. BP, a direct bandgap 2-D semiconductor whose bandgap is thickness-dependent, exhibits extremely in-plane anisotropic features. By patterning monolayer BP into periodic nanostructures or integrated with subwavelength structures, efficient plasmonic resonances can be excited. Anisotropic perfect absorber [117], strong couplings between plasmons [118], and hyperbolic metamaterials [119] can be realized and exhibit active tunability with carrier doping at the mid-IR and THz regions.

The direct bandgap in monolayer TMDs leads to much stronger photoluminescence (PL) [120]. However, the limited light absorption (due to atomically thin thickness) and large nonradiative recombination rate of excitons (far exceeding the radiative recombination rate) result in low PL efficiency (less than 10^{-2}), limiting their applications in practical devices [121]. Fortunately, the integrations of TMDs with metasurfaces, either by transferring TMDs on metasurfaces or patterning metasurfaces on TMDs, offer possible solutions and enable the significant manipulation of the near-field and local optical density of states, resulting in tunability of absorption/emission properties [122], [123]. Recently, a 2000-fold enhancement

in the PL intensity of MoS_2 is achieved by simultaneously enhancing absorption, emission, and directionality of the system [see Fig. 5(a) and (b)] [124], which is around 50 times larger than typical PL enhancement factor (EF) by plasmonic nanoantenna array [125]. By suspending monolayer WSe_2 flakes onto metasurface consisting of sub-20-nm-wide trenches in a gold substrate, a 20 000-fold PL enhancement has been achieved [see Fig. 5(c) and (d)] [126]. Both the excitation and emission processes dominate the PL intensity enhancement. In the excitation process, incidence wavelength matched with the resonance of the metasurface gives rise to an enhanced near field, resulting in the increase of excitation rate of electron-hole pairs in WSe_2. In the emission process, the metasurface enhances the spontaneous emission rate of WSe_2 via the Purcell effect.

The optical cavity can further improve the valley polarization of PL. Namely, the handedness of the PL can be controlled by the polarization of the incident light. The phenomenon of valley polarization originates from inversion asymmetry and strong spin–orbit coupling in monolayer TMDs, leading to spin-valley locking at the direct bandgap valleys [127]–[129]. The valley polarization degree is dramatically decreased at room temperature owing to the large intervalley scattering, which can be ameliorated by incorporating TMDs with metasurfaces. Valley-polarized exciton polaritons have been observed in monolayer MoS_2 embedded in a planar microcavity [see Fig. 5(e) and (f)] [130] and in monolayer WS_2 coupled to cavity photons [131] at room temperature. The PL spectra of TMDs are generally dominated by excitons, i.e., electron-hole pairs bound by Coulomb force. The excitons in monolayer WS_2 can be optically bright or dark according to the spin configuration of electrons and holes [132]. The dark excitons have much longer radiative lifetime than bright excitons because the parallel electron-hole spin momentum is not conserved, which may be used to create "fast" or "slow" light. Direct detection of dark excitons has been observed in monolayer WSe_2 by placing it on top of a single-crystalline silver film [see Fig. 5(g) and (h)] [133]. The near-field coupling of WSe_2 to surface-plasmon polaritons improves the experimental capabilities for probing and manipulating exciton dynamics of atomically thin materials.

Nonlinear properties of TMDs can also be enhanced with optical cavity or plasmonic structures. Around 200-fold SHG enhancement of monolayer WSe_2 by coupling to photonic crystals was demonstrated [134]. Further SHG enhancement ($\sim$3300-fold) was achieved by integrating monolayer MoS_2 with a doubly resonant optical cavity [see Fig. 5(i) and (j)] [135]. Recently, $\sim$7000-fold SHG enhancement of monolayer WSe_2 on sub-20-nm-wide gold trenches on flexible substrates has been reported [see Fig. 5(k) and (l)] [136]. Besides, a synthetic Au–WS_2 metasurface was investigated not only to achieve SHG enhancement (tenfold) but also to steer the nonlinear photons from different valleys to any desired direction in free space at room temperature [137].

IV. PHASE CHANGE MATERIALS

Phase change materials (PCMs) [138] have intrigued an extensive amount of interest in recent years due to their exotic material properties, which can be thermally, optically, electrically, or even mechanically switched. Such exceptional materials have been adopted to realize optically reconfigurable metadevices, which is revolutionizing the data storage industries by affording high-speed, portable, inexpensive, and reliable platforms to store explosive information. In recent years, several promising materials come into our attention: vanadium dioxide (VO_2) [139]–[180] germanium–antimony–tellurium alloy (Ge:Sb:Te, GST) [181]–[196], liquid crystals [197], [198], and gallium [199]. They share the basic yet most important feature in modulating optical response at structured interfaces, i.e., the first-order phase transformation, which induces the change in refractive index, electric conductivity, dielectric constant, and so on. In what follows, we focus on two typical phase change materials (VO_2 and GST) to illustrate their fundamental properties, operation principle, and possible applications for metasurfaces.

A. Vanadium Dioxide

VO_2 is probably the most frequently studied phase change material due to its low transition threshold. The phase transformation undergoes from the insulating phase to metallic phase (IM) above the critical temperature of 340 K ($\sim$67 °C) [139]. More specifically, VO_2 is resistive in the former case, while it is more conductive in the latter case. Prior to intriguing properties and applications of VO_2, the crystallization mechanism and basic physics behind IM transition have been extensively studied [140]–[145], for example, femtosecond structural dynamics [140], coherent structural dynamics [141], near-threshold behavior [142], gate field dependence of metal-insulator transition [143], breaking the crystallization speed limit with a weak electric field and a subsequent stronger electrical pulse [144], and even stabilization of the metallic phase through electric field-induced oxygen vacancy in VO_2 [145]. Explosive studies have demonstrated that the phase transition can be optically [140]–[142], electrically [143]–[145], and thermally [146]–[148] driven. In the former two cases, the triggered electrical current and picosecond/femtosecond pulsed laser convert the electronic and photon energy into thermal counterpart. The optically induced phase transition has been researched over a broad spectral range from millimeter-wave [173], terahertz [141], [142], and infrared [143], [146], [147] to visible [148].

The phase transition and properties of VO_2 can be modulated by doping [149], [150], patterned nanoparticles [146]–[148], and coupling to cavity resonances [151], [152] and nanostructures [153]–[177], [180]. Doping VO_2

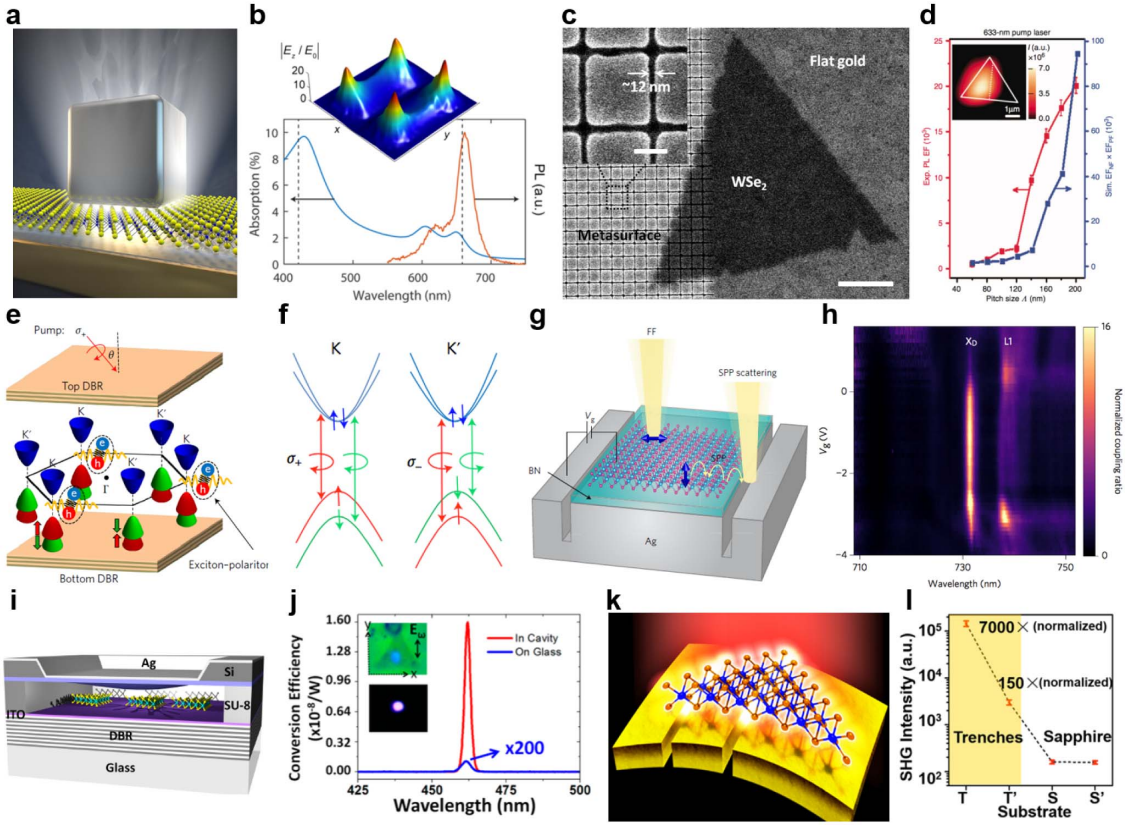

Fig. 5. ***PL and SHG enhancement of TMDs. (a) Schematic of cavity-enhanced PL of MoS2 [124]. (b) Spatial map of the field enhancement across the nanocavity at the second-order mode (top) and optical absorption (blue line) and PL (red line) spectra of monolayer MoS_2 on SiO_2 (bottom) indicating a 2000-fold PL enhancement [124]. (c) SEM image of monolayer WSe_2 covering both metasurface and flat gold [126]. (d) Experimental PL EF (red line) and the simulated EFNF × EFPF (blue line) spectrum indicating a 20 000-fold PL enhancement [126]. Schematic of (e) valley-polarized exciton-polaritons in MoS_2 incorporated into a cavity and (f) valley-spin optical transitions [130]. (g) Schematic of the experimental setup for probing dark exaction emission [133]. (h) Normalized coupling ratio (SPP-PL/FF-PL) as a function of gate voltage [133]. (i) Schematic of monolayer MoS_2 in a doubly resonant on-chip optical cavity [135]. (j) Second-harmonic wave signal indicating a 3300-fold SHG enhancement [135]. (k) Schematic of efficient SHG from ultrathin and flexible hybrid nanostructure of monolayer WSe_2 on metasurface [136]. (l) SHG peak intensity of WSe_2 on gold trenches and on sapphire indicating a 7000-fold SHG enhancement [136]. Scale bar is 100 nm in the inset of (c) and 1 μm in (c).***

degrades the transition temperature and adjusts the transition property such as hysteresis in a reversible manner. Hydrogen doping [149] and interfacial doping with Ti in a core–shell scheme [150] are common methods. By patterning VO_2 nanoparticles, the hysteresis width shows narrower with increasing size of VO_2 nanoparticles and the heterogeneous nucleation process at the nanoscale triggered by oxygen vacancy defects gives rise to the IM phase transition [148]. The phase transition temperatures of VO_2 nanoparticles can even be lower by optimizing preparation process, size, and shape [147]. Coupling ultrathin VO_2 film with sapphire substrate has yielded a perfect absorption [151] because of its large imaginary part of refractive index at intermediate state in the IM phase transition. The ultrafast IM transition VO_2 enables to control the spontaneous light emission of a quantum emitter [152].

The interaction of nanostructures with VO_2 has been comprehensively studied in active metasurfaces and plasmonic systems, demonstrating substantial advantages and applications [153]–[177], [180]. Au nanoparticle covered by VO_2 film was employed to inspect the blueshift of localized surface-plasmon resonance [153]. SRRs [154] or Y-shaped antenna [155] stacked on VO_2 realized the redshift of both permittivity and permeability after IM phase transition. A similar strategy has been demonstrated on reflected phase change [156], broadband dynamic control ranges [157], and large amplitude modulation [158]. The dynamic tuning of frequency response can be utilized for memory use. As shown in Fig. 6(a), by attaching a voltage pulse on electrodes connected to two sides of in-plane SRR array fabricated on a thin VO_2 film, hysteretic resistance behavior and drastic redshift of resonance are clearly observed during a complete temperature cycle [159]. The nanoscale interplay of IM phase transition of VO_2 and plasmonic hysteresis has been demonstrated, while the volume of VO_2 is contained within the SRR gap [see Fig. 6(b)] [160]. The plasmon resonance of nanoparticles establishes an efficient avenue in assisting optical excitation with low-power laser-induced or low-temperature switching. This configuration

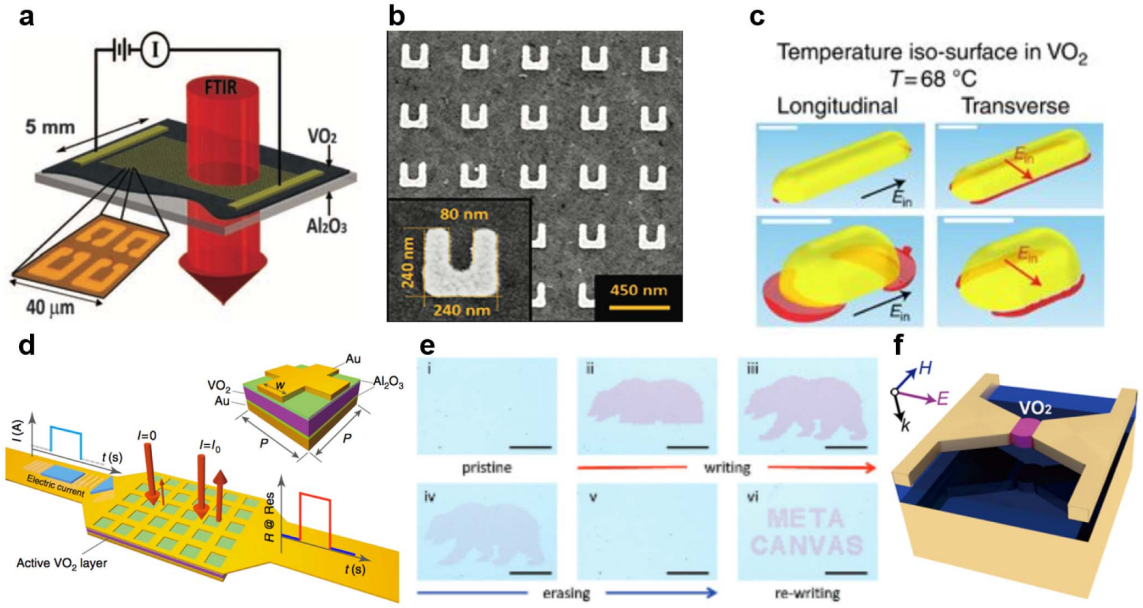

Fig. 6. ***Modulation of nanostructures with VO_2. (a) Memory metamaterials as hybrid system consisting of an SRR array on a VO_2 film [159]. (b) Detecting nanoscale size dependence with VO_2 contained within the SRR gap [160]. (c) Antenna-assisted picosecond control of nanoscale phase transition in VO_2 [170]. (d) Electrically triggered multifunctional control [171]. (e) Writing and erasing process on the field-programmable photonic metacanvas [177]. (f) VO_2-assisted bowtie antenna for dynamically reconfigurable metadevice [180]. Scale bars are 100 nm in (c) and 100 μm in (e).***

overcomes the Coulomb potential barrier for IM phase transition of VO_2 [161] and induces hot-electron injection-driven ultrafast phase transition [162]–[164] and nonresonant plasmonic heating [165]–[167]. Strikingly, the enhanced modulation range and the lowered IM transition temperature were realized by employing hybrid nanogap-VO_2 through thermal [168] or terahertz-pulse [169] excitation. Recently, the antenna-VO_2 hybrid manifests thermal memory for both pulsed excitation by altering optical pumping repetition rate and temperature change [see Fig. 6(c)] [170]. The utilized pulse energy of the antenna-assisted system has successfully lowered by 20 folds. There are some applications based on the aforementioned properties, such as electrical switching of reflectance [see Fig. 6(d)] [171], electrically tuning the wavefront of the gradient transmissive metasurface [172], [173] and reflective metasurface [174], electrically modulating the polarization state of light [175], [176], rewritable metacanvas [see Fig. 6(e)] [177], dynamic color generation [178], and reconfigurable modulation of polariton wave [179]. As fast as 1.27 ms, electrically tunable optical modulators have been demonstrated with a bowtie field antenna to avoid a large thermal mass of continuous film [see Fig. 6(f)] [180].

B. Germanium–Antimony–Tellurium Alloy

Although VO_2 exhibits low transition threshold, the resonance shift and spectrum contrast are trivial at NIR frequencies, because the complex refractive index of VO_2 changes significantly in imaginary part but slightly in real part during the phase transition. GST film affords an alternative possibility to solve the above-mentioned issue and has experienced an exponential growth of interest in recent years [181], [182]. It typically contains two phase states that can be reversibly switched: amorphous state and metastable cubic crystalline state. The crystalline-to-amorphous transition can be actualized by a melt-quenching process requiring a short (nanosecond level), high-repetition-rate laser pulse that quickly raises the temperature above the melting point of $T_m \approx 600$ °C. However, the transition from amorphous to crystalline state is an annealing process that requires a longer, lower intensity pulse to preserve the material above its crystallization temperature $T_c \approx 160$ °C for a short time. Between amorphous and crystalline states, the huge contrast of dielectric properties is present. The resultant change in a refractive index brings about substantial changes in spectral dispersion of the resonances, transmissions, and reflections, especially at wavelengths close to the resonance. GST has been widely exploited and commercialized in rewritable optical disk storage and nonvolatile electronic memories due to its good thermal stability, high switching speed, and large number of achievable rewriting cycles.

The switchable optical properties of plasmonic antenna [183], [184], metamaterials [185]–[187], and metasurfaces [188] were demonstrated by the integration with GST film. The Al nanoantenna covered by an extremely thin GST film was reported to switch infrared plasmonic resonances assisted by femtosecond laser

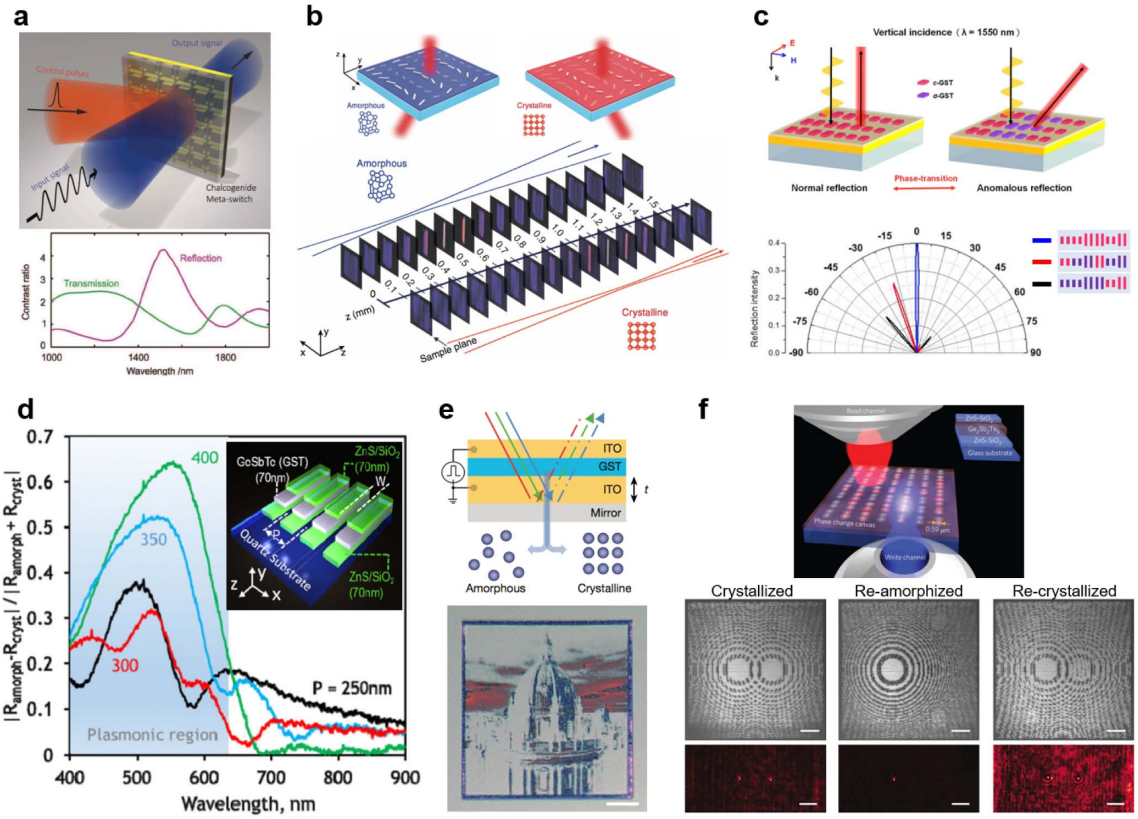

Fig. 7. ***Switchable and reconfigurable devices based on GST. (a) Hybridized GST films with plasmonic metamaterial for optical resonance switching (top) and transmission and reflection modulation contrast (bottom) [185]. (b) Opposite beam switching and bifocal lensing with different foci of the active plasmonic metasurface [188]. (c) Patterned GST nanostructures for active dielectric metasurface (top) and its tunability demonstration: tunable gradient metasurface (bottom) [191]. (d) Relative reflection changes of phase-change-driven dielectric-plasmonic transitions in GST metasurfaces [192]. (e) Reconfigurable color display devices based on the GST film (top) and the electrically constructed image (bottom) [193]. (f) Reconfigurable GST-based metasurfaces (top) and the dynamically optically reconfigurable zone-plate device (middle and bottom) [196]. Scale bars are 10 μm in (e) and (f).***

pulses [183]. Such switching of resonance is marked, nonvolatile, and reversible due to the phase transition properties of GST. The GST can be utilized as an NIR optical switch by inserting a short section of GST to bridge two parts of a bowtielike metallodielectric dimer nanoantenna [184]. The significant variations and shifts of plasmonic resonance peaks between pulse-induced amorphous and crystalline phases qualify it as a switch platform. The GST films were hybridized with plasmonic structures for optical resonance switching [see Fig. 7(a)] [185], switchable perfect absorber [186], and switchable chirality [187].

Massive switch contrast arises in the transmission and reflection rate, which is ascribed to their dielectric constant or refractive index change induced by amorphous–amorphous state transition [185]. The amorphous and crystalline dual-phase state of GST can be utilized to multiplex different functionalities by interleaving two different types of metaatoms in a metasurface to demonstrate bifocal zoom lensing [see Fig. 7(b)] [188]. Two rows of antennas were alternated to impart different geometric phases, resulting in bifunctional devices with independent design. In each phase state, the incident light only interacts with one type of antenna.

The patterned GST nanostructures can also realize optically switchable resonance shifter [189], [190] and phase shifter [191], [192]. The dramatic change of optical contrast of the patterned GST sphere in amorphous and crystalline phases was demonstrated to shift the mode between an electric dipole resonance and an anapole state [190]. The nanostructured GST was employed as a basic building block of the metasurface in the NIR spectrum rather than a background medium. By using GST rods as the basic unit and controlling the crystallization fraction of GST rods, the variable optical resonance of metaatom, multilevel phase, and wave modulation can be engineered in its amorphous and crystalline states [see Fig. 7(c), top] [191]. Tuned Fano resonances and anomalous reflection beam steering can be modulated [see Fig. 7(c), bottom]. Dielectric-plasmonic transitions in switchable GST metasurfaces were demonstrated [see Fig. 7(d)] [192]. By stimulating the GST nanograting metasurface with a different number of laser pulse, repetition rate, and energy of the pulse, a positive-to-negative dielectric constant of

GST is manifested. The GST metasurface transforms from dielectric to plasmonic state from ultraviolet to visible spectral range, enabling large switching contrast of reflections, transmissions, and color change [192].

Electrically or optically patterning GST film can realize reconfigurable devices, such as color display [193], [194], hologram [195], and metasurfaces [196]. In this scheme, the GST film was typically encapsulated between two thin films (e.g., ITO or ZnS–SiO_2), which were protected against atmospheric degradation. As shown in Fig. 7(e), the GST film is sandwiched between top-and-bottom ITO layers [193]. By changing the direct current attached to the electrode and tailoring the thickness of the bottom ITO spacer (crucial factor) and GST layer, reflectivity (color) is modulated at specific wavelengths when illuminated by white light. Then, by cautiously selecting above-mentioned nanostructured films as pixels, electrically tunable color display devices can be actualized [see Fig. 7(e), bottom]. The reflective color display device can be readily extended to a transmission scheme by removing the mirror [193]. Such ITO-GST-ITO composite metaatom was later adopted to realize a full-color digital computer-generated hologram by varying the pulse energy illuminated on the hologram without damaging the bottom Al and ITO layer [195]. Optically reconfigurable GST-based metasurfaces have been demonstrated with the continuously controlled degree of multilevel crystallization on GST film sandwiched between ZnS–SiO_2 layers [see Fig. 7(f), top] [196]. Dynamically reconfigurable focusing lens with different numbers of foci can be engineered based on a write–erase–write reconfiguration cycle process, i.e., selective crystallization and reamorphization [see Fig. 7(f), middle and bottom].

V. CARBON GROUP, III–V SEMICONDUCTORS, AND DIELECTRIC MATERIALS

Thanks to the low loss in visible frequency, many high-index dielectric materials have been widely utilized in the design of metasurface. The strong electric and magnetic resonances excited inside the dielectric metaatoms bring advanced functionality. The main choices of dielectric materials in the visible and NIR range are silicon (Si), titanium dioxide (TiO_2), gallium nitride (GaN), gallium arsenide (GaAs), germanium (Ge), and other semiconductors with high refractive index and low loss. There are mature technologies to process these materials in current device technologies and foundries. There are some other metasurfaces made of or integrated with different semiconductors, such as lead telluride (PbTe) metasurface for thermal-optic tuning [200] and indium antimonide (InSb)-based heterojunction for analogous voltage-dependent phase shifts [201] in the midinfrared region. By virtue of few reports on metasurfaces integrated with these semiconductors, in what follows, we focus on the typical materials (graphene, TMDs, and BP) to illustrate their fundamental properties, operation principle, and possible applications for metasurfaces.

As a high-refractive-index semiconductor, silicon has been applied in a vivid structural color generation. Via oxidation of silicon antenna, an oxide film can be deposited on the surface and leads to the geometrical changes of these antennas, which facilitate to shift the Mie resonance wavelength and change the structural colors consequently [202]. Based on this condition, monocrystalline Si nanopatch arrays were fabricated and the generated structural colors can be tuned from red to blue by the oxidation of each nanopatch [see Fig. 8(a)]. Instead of modifying the optical properties of the materials in dielectric metasurface, Sun *et al.* [203] reported a tunable structural color spanning the entire visible spectrum with microfluidic reconfigurable TiO_2 metasurfaces by changing the refractive index of the surrounding medium. Fig. 8(b) shows the color of word "HIT" and its background varies with the different surrounding refractive index. Once the CS_2 was injected to the polymeric microfluidic channel, the encoded information can be erased. The color transition time is less than 16 ms, far smaller than previous reports. Moreover, the structural colors can also be controlled by varying the polarization degree of the incident light. The polarization-sensitive TiO_2 metasurface has been experimentally demonstrated, which can realize three-primary-color switching [204]. In Fig. 8(c), it shows that the structural colors change a lot when polarization angles change from 0° to 90°, e.g., green-color metasurface at x-polarization switched to blue at y-polarization. Furthermore, dynamic color display can also be achieved via the combination of extrinsic structural color and intrinsic emission color. Gao *et al.* [205] demonstrated an *in situ* reversible color nanoprinting paradigm via photonic doping, triggered by the interplay of structural colors and photon emission of MAPbX3 gratings [see Fig. 8(d)]. The presented color could be tuned by modifying the emission intensity, which is determined by the external pumping light density. Apart from resonance shifting for color application, dielectric metasurfaces were also demonstrated static phase control in the NIR (Si) [206] and visible (TiO_2 and GaN) [6], [207] spectrum for application of metalens [6], [207], [208], spin-to-orbital converter [9], [209], [210], full-color routing [211], and light-field imaging [212]. The metasurfaces mentioned earlier are mainly made of active materials. However, they are failed to demonstrate dynamic, tunable, or reconfigurable modulation.

The combination of Si metasurface with microelectromechanical systems (MEMS) provides another approach to modify the functionality of metasurface device. Arbabi *et al.* [213] proposed and demonstrated a silicon metasurface doublet with electrically tunable focal distance. The designed tunable lens is composed of a stationary lens on a substrate and a moving lens on a membrane. By applying different voltages, the distance between two lenses can be modified at will and the absolute efficiency

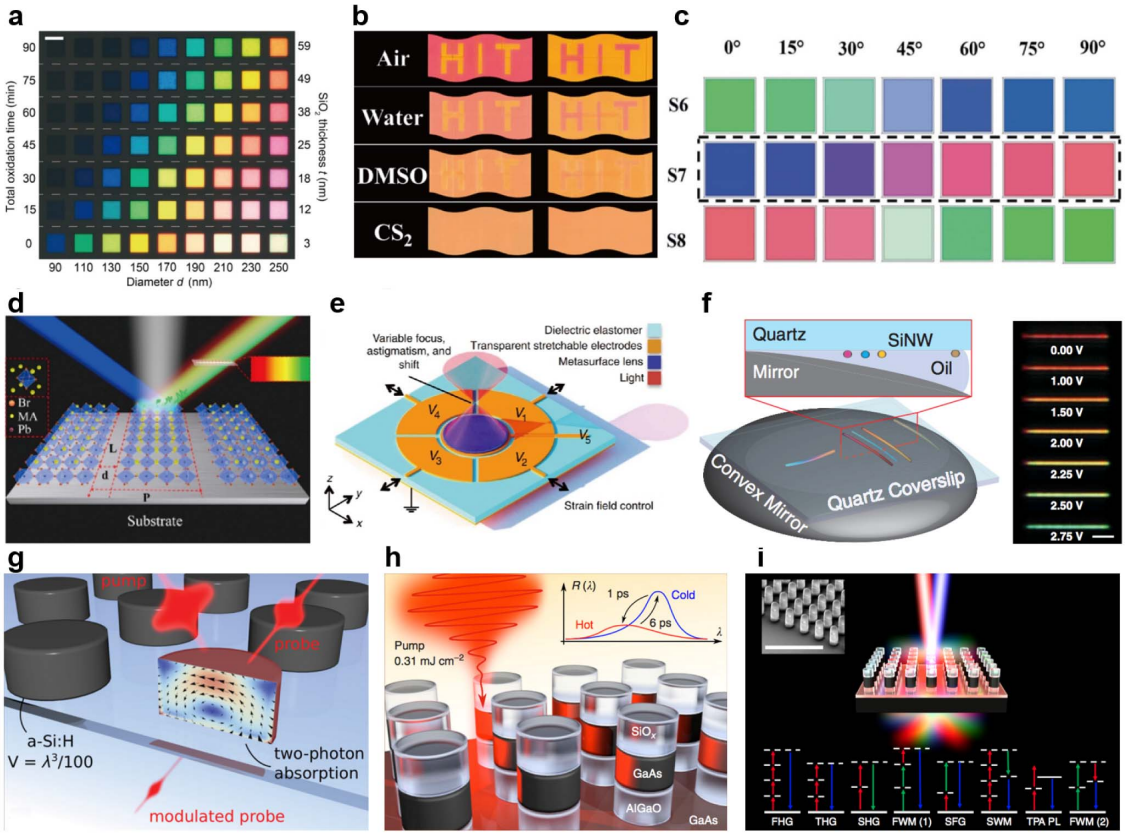

Fig. 8. ***Si-, TiO_2-, GaAs-, and Ge-based active metasurfaces. (a) Reflection image of oxidized arrays irradiated with linear polarized white light [202]. With the increased oxidation time, the structural colors blue shift. (b) Bright-field photographs for two samples in different solvents [203]. With the increase of surrounding refractive index, the encoded information can be fully concealed. (c) Structural colors varied with the polarization angles of incident light in a step of 15° [204]. (d) Schematic design of pixels and the in situ color generation by mixing extrinsic structural color and intrinsic emission color on MAPbX3 perovskite gratings [205]. (e) Schematic of the device that is combined with metalens and dielectric elastomer actuators [214]. (f) Configuration of the Si nanowire (left) and its dark-field images at each bias putting in the NEMS platform (right) [215]. (g) Illustration of ultrafast all-optical switching in resonant silicon nanodisks [216]. (h) Schematic of ultrafast and high-efficient all-optical tuning of GaAs metasurface [218]. (i) Schematic of an optical metasurface mixer consisting of a square array of subwavelength GaAs dielectric resonators and the SEM image (inset) [219]. Scale bar is 10 μm in (a), 2 μm in (f), and 3 μm in the inset of (i).***

is more than 40% for all voltage values. Notably, the metasurface doublet is correctly designed that a small change in the distance between two lenses leads to a significant change in the focal length. Instead of tuning based on longitudinal motion, lateral control of metalens can also be utilized to vary focus and magnification. She *et al.* [214] combined metasurface optics with dielectric elastomer actuators (also called artificial muscles in soft robotics) to realize an electrically tunable device. By applying different voltages, the focal length can be directly tuned, resulting from the lateral expansion or contraction of postspacing [see Fig. 8(e)]. Holsteen *et al.* [215] achieved a strong dependence of the optical properties of Si nanowires on the external environment. The resonance and scattering of Si nanowire shifts across a large part of the visible spectrum, while it puts above an aluminum mirror at different heights [see Fig. 8(f), left]. A nanoelectromechanical system (NEMS) platform was further developed to actively tune the scattering intensity and spectral properties of a Si nanowire to achieve active tuning of light scattering at 1 MHz [see Fig. 8(f), right]. Furthermore, by activating different combinations of electrodes, other functionality, such as astigmatism and image shift, can also be realized.

Another degree of freedom to tailor the performance of metasurfaces is the nonlinear response. One significant nonlinear characterization is that the refractive index of semiconductor could be modulated via the injection of free carriers. When integrated with metasurface, the nonlinear-optical properties were found to be orders of magnitude stronger than that of the constituent material. For instance, all-optical ultrafast switching can be achieved by utilizing enhanced two-photon absorption (TPA) in hydrogenated amorphous silicon (a-Si:H) metasurface [see Fig. 8(g)] with a depth of 60%, switching time as low as 65 fs [216], and full recovery to zero within about 20 ps [217]. As a direct-gap semiconductor with large nonlinear susceptibilities, GaAs is a material for all-optical modulation and active metasurface more attractive than silicon, a kind of

indirect semiconductor. Shcherbakov *et al*. [218] realized the ultrafast and high-efficient all-optical tuning of GaAs metasurface based on ultrafast injection and relaxation of free carriers for the first time. Under low pump fluence value, the absolute reflectance tuning of up to 0.35 and the spectral position tuning of the MD resonance up to $\lambda = 30$ nm were demonstrated [see Fig. 8(h)] due to generated free carriers. Nonlinear optics vastly extends the functionality of metasurface and makes it possible to integrate more functionalities into a single optoelectronic device. Liu *et al*. [219] experimentally demonstrated a GaAs metasurface that generates seven different nonlinear optical processes, which include second-harmonic, third-harmonic, and fourth-harmonic generation, sum-frequency generation, TPA-induced PL, four-wave mixing, and six-wave mixing, occurring simultaneously [see Fig. 8(i)].

VI. DIODE IN MICROWAVE REGION

Microwave region is also a common frequency band of EM wave, to which metamaterial and metasurface research has devoted [220], [221]. Wide potential applications about active metasurfaces in microwave, such as radio and microwave transmission, are to be developed. Since the size of metaatoms in the microwave region is relatively larger and easier to demonstrate, the development of active metasurface in this region about regulatory approaches is earlier than that of visible and infrared region. Some concepts in the microwave region might be useful in the visible and infrared region. The active metasurface can be realized by combination with active devices, such as transistors and varactor diodes, which are typically useful for microwave manipulation. There have been some interesting developments of active metasurfaces that can switch functions based on diode operating in the microwave region, such as microwave absorbers, cloaks, scattering modulation, and polarization converters. Microwave absorbers have drawn significant attention in recent 20 years for its wide application values. An electrically active absorber in the microwave frequency was designed and presented, in which the dividable frequency and amplitude modulation on active magnetic resonator can be respectively controlled by varactor and pin diodes [see Fig. 9(a)] [222]. For the application of cloaks, previous passive cloaks can only function for geometry-specific objects as well as preset phase profile and surface profile. A reconfigurable carpet cloak based on active metasurface was presented in [223]. By controlling the bias voltage of varactor diodes loaded on the metasurface, the surface phase distribution can be dynamically tuned and, hence, the cloak will change the scattering fields as predesigned.

For the application of polarization converters, it is possible to switch the functions among various polarizations in a wideband [224]. A reconfigurable and broadband reflective polarization converter was designed with metaatom composed of a butterfly-shaped antenna embedded with a varactor diode and a dielectric substrate backed with a modified metal ground [see Fig. 9(b)] [225]. The active metasurface imposes the difference phases for two orthogonal polarizations of the incidence and controls the polarization states of the reflected waves. When applying bias at 0 V, the device acts as a linear polarization converter, rotating a linearly polarized wave to its cross-polarized direction in a wideband. In contrast, the device acts as a circular polarization converter when applying bias at t19 V. The other reconfigurable conversion was demonstrated to switch different functions, such as reflections, transmissions, and polarizations of EM waves [226]. It is composed of two metallic layers with a middle dielectric layer in between. The top metallic layer is designed as periodic metallic short wires to convert linear polarized incidence into its orthogonal direction (OFF state). The bottom metallic layer connected to pin diodes can reflect the incidence, while the pin diodes switch ON (ON state).

Comparing with the reflection-type tunable metasurfaces [227], [228], transmission-type metasurfaces face the challenge of relatively low efficiency and limited phase coverage. Huygens' metasurface is known to provide full 2π-phase coverage with high manipulation efficiency by suitably engineering both electric and magnetic polarizabilities of the metaatoms [221]. A reconfigurable Huygens' metasurface was realized by loading active elements in resonating metaatoms, and hence, the metasurface can tune the transmission amplitude and phase responses simultaneously, showing complex focal spots at distinct spatial positions [see Fig. 9(c)] [229]. These multiple focal spots can be moved along predesigned trajectories with high efficiency and fast response time, by changing the control voltage applied to the varactors.

The next milestone for diode-based active metasurface is to achieve full modulation of phase/amplitude/polarization at individual pixels or metaatoms. In this connection, Cui *et al*. [230], Li *et al.* [231], [232], Zhang *et al.* [233], [234], Zhao *et al.* [235], and Zhang *et al.* [236] proposed the binary digital coding metasurfaces that are composed of only two types of unit cells named as "0" and "1" elements within opposite phase responses (π phase different) for 1-bit coding [230]. Such metasurfaces can be controlled in a digital way by using the field-programmable gate array (FPGA). Therefore, the programmable metasurface can be realized to manipulate EM waves in real time by programming different coding sequences with 2-bit coding or higher. A single metasurface can thereby accomplish various functions via FPGA, such as single-sensor and single-frequency imaging [231] and reprogrammable holograms with modulation time around 33 ns [see Fig. 9(d)] [232]. One can also control various functions of digital coding metasurfaces by light. Light-controllable digital coding metasurface has been proposed and designed to tune the reflection phase as desired by changing the intensity of the illumination light [233]. Moreover, the digital coding metasurface can numerically achieve free switches of the transmission status in two different manners by remotely tuning the

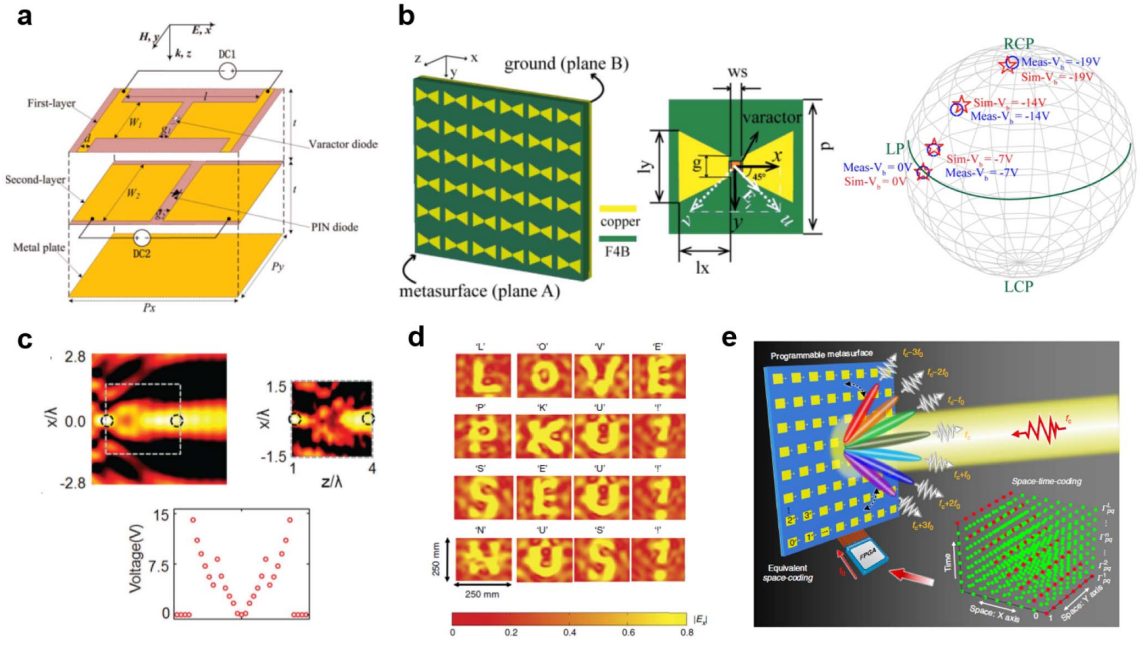

Fig. 9. ***Diode-based metasurfaces. (a) Illustration of the active microwave absorber [222]. (b) Active polarization converter (left and middle) and generated polarization states on the Poincare sphere (right) [225]. (c) Two foci for distinct positions [229]. (d) Experimentally observed holographic images [232]. (e) Space–time coding digital metasurface [236].***

illumination intensity or shifting the frequency of the incident wave [234].

Furthermore, the digital coding metasurface can be extended from the space domain to the frequency and time domains. Recently, a dynamic time-domain digital coding metasurface was introduced to enable efficient manipulations of spectral harmonic distributions [235]. Driven by different combinations of output voltages from FPGA, the metasurface can implement many functions by controlling the time-domain digital coding states. The idea of space–time modulated digital coding metasurface was proposed to obtain simultaneous manipulations of EM waves in both space and frequency domains [see Fig. 9(e)] [236]. Hence, the EM metasurface can exert control to the spatial beams and harmonic power distributions simultaneously.

VII. CONCLUSION

In the last few years, remarkable progress has been made in semiconductor-based active metasurfaces or devices thus far. It is important to outline the difference in modulation speed, tuning mechanism, and operational wavelength across different semiconductor candidates. Different types of materials and the modulation methods (mainly focus on electrical and optical tuning) and properties mentioned in this paper are compared in Table 1. Based on the comparison shown in Table 1, one can identify the most suitable semiconductors to realize a designer metasurface, and our review may help as a timely guide.

The modulation speed of nonlinearity of these materials is relatively faster than other modulation methods. As fast as 65 fs of switching time has been demonstrated in a-Si:H-based Huygens' metasurface [216]. As a comparison, from subpicosecond to few picoseconds, switching time has been investigated in TCO- and GaAs-based metasurfaces [50], [52], [55], [56], [218]. Considering the electrical modulation, graphene-based metasurface can get repetition rate up to tens of gigahertz [99], faster than that of the p-i-n diode (hundreds of megahertz) [232] and ITO-based (few megahertz) [38] metasurfaces. However, their main operation frequency regions are different. ITO-based metasurfaces are mainly in the NIR and midinfrared region [36], [38], [40]. While graphene and p-i-n diode-based metasurfaces are mainly in the midinfrared-to-far-infrared [106], [107] and microwave regions [225], [231], [232], [236]. As a comparison, although the crystallization speed of VO_2 can achieve as fast as 500 ps [144], the repetition rate of VO_2-based metasurface that can get is around hundreds of hertz operating in the visible and NIR region [180]. In contrast to the other PCMs, GST-based metasurfaces can get faster repetition rate similar to ITO based (few megahertz) and operate in the NIR region but are usually tuned by optical modulation [185], [188], [192]. In addition, the metasurface can modulate the fast optical processes in TMDs, such as light absorption and emission with the related exciton lifetime of tens of picosecond in MoS_2 [237]. The metasurface-enhanced optical spectra of TMDs are generally in the visible-light range [124], [126], [135], [136].

About the dynamic transmission/reflection phase modulation, ITO and graphene-based gate-tunable metasurfaces achieve around $3\pi/2$, respectively, operating in NIR and midinfrared [40], [106], [107]. Varactor diode-based metasurfaces can get near 2π phase modulation in the microwave region [229]. The coding

Table 1 Comparison of Different Mechanisms

Material type	Material	Operation spectrum	Tuning Mechanism	Modulation speed or repetition rate	Modulation and range
1. TCOs	ITO	NIR - MIR	Electrical	100 kHz - 10 MHz	Reflectance: $\Delta R/R$ = 35% [36]
					Reflectance: ΔR = 89% [40]
					Reflection phase: 303° [40]
			Optical	~ 1 ps	Nonlinearity: ΔOD = -0.37 and $\Delta T/T$ = 134% [52]
					Nonlinearity: n_2 = 3.73 cm^2/GW, β = 2160 cm/GW [56]
	CdO:In	NIR - MIR	Optical	~ 1 ps	Nonlinearity: ΔR = 85.3% and polarization extinction ratio = 91 [55]
2. 2D Materials	Graphene	MIR - FIR	Electrical	30 MHz - 20 GHz	Transmittance: $\Delta T/T$ = 100% [97]
					Absorption: ΔA = ~ 100% [99, 102]
					Reflection phase: ~240° [106, 107]
			Optical	~ 1 min	Transmittance: $\Delta T/T$ = 5% [90]
	MoS_2	VIS	Optical	NA	PL intensity 2,000 fold [124]
					SHG intensity 3,300 fold [135]
	WSe_2	VIS	Optical	NA	PL intensity 20,000 fold [126]
					SHG intensity 7,000 fold [136]
3. PCMs	VO_2	NIR-MIR	Electrical	1 ms - 500ms	Resonance wavelength: $\Delta\lambda$: ~360 nm and $\Delta\lambda/\lambda$: ~33% [180]
					Reflectance: ΔR = 80%, $\Delta R/R$ = 75% [171]
					Reflection Phase: 180° [174]
	GST	VIS-NIR	Optical	~100 ns ~ 1 MHz	Resonance wavelength: $\Delta\lambda$: ~200 nm and $\Delta\lambda/\lambda$: ~30% [185]
					Focal length: Δf = ~0.5mm and $\Delta f/f$ = ~50% [188]
					Transmittance: ΔT = ~23% and $\Delta T/T$ = ~65.7% [192]
4. Carbon group, III-V semiconductors, etc.	Perovskite	VIS	Optical	NA	Resonance wavelength: $\Delta\lambda$ = ~ 100 nm and $\Delta\lambda/\lambda$ = ~19% [205]
	a-Si w/ MEMS	NIR	Electrical	NA	Focal length: Δf = ~ 200 μm and $\Delta f/f$ = ~ 30% [213]

Table 1 *(Continued.)* Comparison of Different Mechanisms

	a-Si w/ DEA	NIR	Electrical	NA	Focal length: Δf = ~ 53.5 μm and Δf/f = ~ 107% [214]
	a-Si:H	NIR	Optical	65 fs	Transmittance: ΔT = ~ 60% [216]
	GaAs	NIR	Optical	1 ps - 10 ps	Reflectance: ΔR = ~ 35% and ΔR/R = ~ 73% [218]
5. Diodes	Varactor diode	Microwave	Electrical	1 kHz - 1000 kHz	Reflection phase: ~320° [223]
					Transmission phase 350° [229]
					Reflection phase: 285° and time-coding [235]
	PIN diode	Microwave	Electrical	100 kHz - 100 MHz	Reflection phase: ~260°and 1-bit coding [232]
					Transmission phase: ~100° and 2-bit coding [231]
					Space-time-coding [236]
					Polarization conversion ratio 80% [225]
	PIN photodiode and varactor diode	Microwave	Optical	NA	Reflection phase 180° [233]
					Transmittance: ΔT = 88.5% and ΔT/T = 93.3% [234]

methods, such as 2-bit coding and space–time coding developed in diode-based metasurfaces, provide a path that other phase modulation metasurfaces can investigate in the future. Mature display technology also provides a path that can individually modulate each metaatom for further possible spatial light modulation.

Although great progress has been made in this field thus far, we realize that this is just the beginning of its rapid development. There are still some challenges and topics for present active metasurfaces that need to be explored.

1) *Performance:* The tuning range and depth of active metasurfaces are usually smaller than passive metasurfaces. There is still room for improvement through judicious designs and new materials.
2) *Tolerance:* The hybridized metasurfaces with semiconductors may require more stringent fabrication process. Taking field-effect configuration for example, the quality of the insulator is very crucial for the measurement, posing more difficulty in the high-quality fabrication process. More accurate subwavelength pixel independent control, more compact integration and interconnection of the devices are essential for completing and promoting the functionalities and performances.
3) *Phase Control:* Some mechanisms have not demonstrated the decent phase modulation yet. For instance, the optical modulation of TCOs has subpicosecond modulation speed, but the difficulties in design and measurement limit the phase modulation demonstration with such high speed. Besides, for most of the present devices, at the same time of phase control, the modulation efficiencies always keep low, which significantly hamper the practical applications.
4) *Working Band:* Adequate studies are still needed for devices working in the visible range, where the active functionalities for most of the traditional semiconductors cannot cover but in heavy demand.

Considering the recent achievements in passive metasurfaces, structured semiconductor interfaces may be inspired from its passive counterparts, such as arbitrary polarization basis [206], [238], dispersion engineering [207], [239], [240], and topology optimization [241]–[243]. On the other hand, the more

advanced semiconductor device-making technologies and synthesis and discovery of novel materials are of great importance for light manipulation with active semiconductor interfaces. The cooperated progress in multidisciplinary sciences (materials, optics, synthesis, and fabrication) lays promising pavements of active metasurface toward nanoscale spatial light modulators, high-resolution display and LIDARs, on-chip devices, and active elements as replacement or assistance in optical systems. ■

REFERENCES

[1] N. Yu and F. Capasso, "Flat optics with designer metasurfaces," *Nature Mater.*, vol. 13, pp. 139–150, Jan. 2014.

[2] L. Zhang, S. Mei, K. Huang, and C.-W. Qiu, "Advances in full control of electromagnetic waves with metasurfaces," *Adv. Opt. Mater.*, vol. 4, no. 6, pp. 818–833, 2016.

[3] H.-H. Hsiao, C. H. Chu, and D. P. Tsai, "Fundamentals and applications of metasurfaces," *Small Methods*, vol. 1, no. 4, 2017, Art. no. 1600064.

[4] S. M. Kamali, E. Arbabi, A. Arbabi, and A. Faraon, "A review of dielectric optical metasurfaces for wavefront control," *Nanophotonics*, vol. 7, no. 6, pp. 1041–1068, 2018.

[5] N. Yu *et al.*, "Light propagation with phase discontinuities: Generalized laws of reflection and refraction," *Science*, vol. 334, no. 6054, pp. 333–337, Oct. 2011.

[6] M. Khorasaninejad and F. Capasso, "Metalenses: Versatile multifunctional photonic components," *Science*, vol. 358, Dec. 2017, Art. no. eaam8100.

[7] M. L. Tseng *et al.*, "Metalenses: Advances and applications," *Adv. Opt. Mater.*, vol. 6, Sep. 2018, Art. no. 1800554.

[8] G. Zheng, H. Mühlenbernd, M. Kenney, G. Li, T. Zentgraf, and S. Zhang, "Metasurface holograms reaching 80% efficiency," *Nature Nanotechnol.*, vol. 10, pp. 308–312, Feb. 2015.

[9] R. C. Devlin, A. Ambrosio, N. A. Rubin, J. P. B. Mueller, and F. Capasso, "Arbitrary spin-to–orbital angular momentum conversion of light," *Science*, vol. 358, pp. 896–901, Nov. 2017.

[10] H. Pahlevaninezhad *et al.*, "Nano-optic endoscope for high-resolution optical coherence tomography *in vivo*," *Nature Photon.*, vol. 12, pp. 540–547, Jul. 2018.

[11] S. Colburn, A. Zhan, and A. Majumdar, "Metasurface optics for full-color computational imaging," *Sci. Adv.*, vol. 4, Feb. 2018, Art. no. eaar2114.

[12] G.-Y. Lee *et al.*, "Metasurface eyepiece for augmented reality," *Nature Commun.*, vol. 9, Nov. 2018, Art. no. 4562.

[13] S. Lan *et al.*, "Metasurfaces for near-eye augmented reality," *ACS Photon.*, vol. 6, pp. 864–870, Mar. 2019.

[14] K. Liu, C. R. Ye, S. Khan, and V. J. Sorger, "Review and perspective on ultrafast wavelength-size electro-optic modulators," *Laser Photon. Rev.*, vol. 9, no. 2, pp. 172–194, 2015.

[15] M. Lapine, I. V. Shadrivov, D. A. Powell, and Y. S. Kivshar, "Magnetoelastic metamaterials," *Nature Mater.*, vol. 11, pp. 30–33, Nov. 2011.

[16] H.-S. Ee and R. Agarwal, "Tunable metasurface and flat optical zoom lens on a stretchable substrate," *Nano Lett.*, vol. 16, pp. 2818–2823, Mar. 2016.

[17] S. M. Kamali, E. Arbabi, A. Arbabi, Y. Horie, and A. Faraon, "Highly tunable elastic dielectric metasurface lenses," *Laser Photon. Rev.*, vol. 10, pp. 1002–1008, Nov. 2016.

[18] Y.-H. Fu *et al.*, "A micromachined reconfigurable metamaterial via reconfiguration of asymmetric split-ring resonators," *Adv. Funct. Mater.*, vol. 21, pp. 3589–3594, Sep. 2011.

[19] M. Rahmani *et al.*, "Reversible thermal tuning of all-dielectric metasurfaces," *Adv. Funct. Mater.*, vol. 27, Aug. 2017, Art. no. 1700580.

[20] D. Cui, B. Bai, and H.-B. Sun, "Tunable metasurfaces based on active materials," *Adv. Funct. Mater.*, vol. 29, no. 10, 2019, Art. no. 1806692.

[21] A. Nemati, Q. Wang, M. Hong, and J. Teng, "Tunable and reconfigurable metasurfaces and metadevices," *Opto-Electron. Adv.*, vol. 1, no. 5, 2018, Art. no. 180009.

[22] S. V. Makarov *et al.*, "Light-induced tuning and reconfiguration of nanophotonic structures," *Laser Photon. Rev.*, vol. 11, Sep. 2017, Art. no. 1700108.

[23] A. Boltasseva and H. A. Atwater, "Low-loss plasmonic metamaterials," *Mater. Sci.*, vol. 331, no. 6015, pp. 290–291, Jan. 2011.

[24] G. V. Naik, J. Kim, and A. Boltasseva, "Oxides and nitrides as alternative plasmonic materials in the optical range [invited]," *Opt. Mater. Express*, vol. 1, no. 6, pp. 1090–1099, 2011.

[25] G. V. Naik, V. M. Shalaev, and A. Boltasseva, "Alternative plasmonic materials: Beyond gold and silver," *Adv. Mater.*, vol. 25, no. 24, pp. 3264–3294, 2013.

[26] E. Feigenbaum, K. Diest, and H. A. Atwater, "Unity-order index change in transparent conducting oxides at visible frequencies," *Nano Lett.*, vol. 10, pp. 2111–2116, May 2010.

[27] A. Melikyan *et al.*, "Surface plasmon polariton absorption modulator," *Opt. Express*, vol. 19, no. 9, pp. 8855–8869, 2011.

[28] V. J. Sorger, N. D. Lanzillotti-Kimura, R.-M. Ma, and X. Zhang, "Ultra-compact silicon nanophotonic modulator with broadband response," *Nanophotonics*, vol. 1, no. 1, pp. 17–22, 2012.

[29] F. Yi, E. Shim, A. Y. Zhu, H. Zhu, J. C. Reed, and E. Cubukcu, "Voltage tuning of plasmonic absorbers by indium tin oxide," *Appl. Phys. Lett.*, vol. 102, May 2013, Art. no. 221102.

[30] J. A. Dionne, K. Diest, L. A. Sweatlock, and H. A. Atwater, "PlasMOStor: A metal-oxide-Si field effect plasmonic modulator," *Nano Lett.*, vol. 9, pp. 897–902, Jan. 2009.

[31] Z. Lu, W. Zhao, and K. Shi, "Ultracompact electroabsorption modulators based on tunable epsilon-near-zero-slot waveguides," *IEEE Photon. J.*, vol. 4, no. 3, pp. 735–740, Jun. 2012.

[32] H. W. Lee *et al.*, "Nanoscale conducting oxide PlasMOStor," *Nano Lett.*, vol. 14, no. 11, pp. 6463–6468, 2014.

[33] G. T. Papadakis and H. A. Atwater, "Field-effect induced tunability in hyperbolic metamaterials," *Phys. Rev. B, Condens. Matter*, vol. 92, Nov. 2015, Art. no. 184101.

[34] G. T. Papadakis, D. Fleischman, A. Davoyan, P. Yeh, and H. A. Atwater, "Optical magnetism in planar metamaterial heterostructures," *Nature Commun.*, vol. 9, Jan. 2018, Art. no. 296.

[35] Y.-J. Lu *et al.*, "Dynamically controlled purcell enhancement of visible spontaneous emission in a gated plasmonic heterostructure," *Nature Commun.*, vol. 8, Nov. 2017, Art. no. 1631.

[36] J. Park, J.-H. Kang, X. Liu, and M. L. Brongersma, "Electrically tunable epsilon-near-zero (ENZ) metafilm absorbers," *Sci. Rep.*, vol. 5, Nov. 2015, Art. no. 15754.

[37] K. Thyagarajan, R. Sokhoyan, L. Zornberg, and H. A. Atwater, "Millivolt modulation of plasmonic metasurface optical response via ionic conductance," *Adv. Mater.*, vol. 29, Aug. 2017, Art. no. 1701044.

[38] Y.-W. Huang *et al.*, "Gate-tunable conducting oxide metasurfaces," *Nano Lett.*, vol. 16, pp. 5319–5325, Aug. 2016.

[39] J. Park, J.-H. Kang, S. J. Kim, X. Liu, and M. L. Brongersma, "Dynamic reflection phase and polarization control in metasurfaces," *Nano Lett.*, vol. 17, pp. 407–413, Dec. 2017.

[40] G. K. Shirmanesh, R. Sokhoyan, R. A. Pala, and H. A. Atwater, "Dual-gated active metasurface at 1550 nm with wide (>300°) phase tunability," *Nano Lett.*, vol. 18, pp. 2957–2963, Mar. 2018.

[41] S. Sun *et al.*, "High-efficiency broadband anomalous reflection by gradient meta-surfaces," *Nano Lett.*, vol. 12, no. 12, pp. 6223–6229, 2012.

[42] A. Pors, O. Albrektsen, I. P. Radko, and S. I. Bozhevolnyi, "Gap plasmon-based metasurfaces for total control of reflected light," *Sci. Rep.*, vol. 3, Jul. 2013, Art. no. 2155.

[43] T. S. Luk *et al.*, "Enhanced third harmonic generation from the epsilon-near-zero modes of ultrathin films," *Appl. Phys. Lett.*, vol. 106, Apr. 2015, Art. no. 151103.

[44] A. Capretti, Y. Wang, N. Engheta, and L. D. Negro, "Comparative study of second-harmonic generation from epsilon-near-zero indium tin oxide and titanium nitride nanolayers excited in the near-infrared spectral range," *ACS Photon.*, vol. 2, pp. 1584–1591, Oct. 2015.

[45] N. Kinsey, C. DeVault, J. Kim, M. Ferrera, V. M. Shalaev, and A. Boltasseva, "Epsilon-near-zero al-doped ZnO for ultrafast switching at telecom wavelengths," *Optica*, vol. 2, no. 7, pp. 616–622, 2015.

[46] M. Abb, Y. Wang, C. H. de Groot, and O. L. Muskens, "Hotspot-mediated ultrafast nonlinear control of multifrequency plasmonic nanoantennas," *Nature Commun.*, vol. 5, Sep. 2014, Art. no. 4869.

[47] Y. Zhu, X. Hu, Y. Fu, H. Yang, and Q. Gong, "Ultralow-power and ultrafast all-optical tunable plasmon-induced transparency in metamaterials at optical communication range," *Sci. Rep.*, vol. 3, Aug. 2013, Art. no. 2338.

[48] Y. Zhu, X. Hu, H. Yang, and Q. Gong, "Ultralow-power all-optical tunable double plasmon-induced transparencies in nonlinear metamaterials," *Appl. Phys. Lett.*, vol. 104, May 2014, Art. no. 211108.

[49] Y. Zhu, X. Hu, Z. Chai, H. Yang, and Q. Gong, "Active control of chirality in nonlinear metamaterials," *Appl. Phys. Lett.*, vol. 106, Feb. 2015, Art. no. 091109.

[50] M. Z. Alam, I. De Leon, and R. W. Boyd, "Large optical nonlinearity of indium tin oxide in its epsilon-near-zero region," *Science*, vol. 352, pp. 795–797, May 2016.

[51] X. Liu *et al.*, "Quantification and impact of nonparabolicity of the conduction band of indium tin oxide on its plasmonic properties," *Appl. Phys. Lett.*, vol. 105, Oct. 2014, Art. no. 181117.

[52] P. Guo, R. D. Schaller, J. B. Ketterson, and R. P. H. Chang, "Ultrafast switching of tunable infrared plasmons in indium tin oxide nanorod arrays with large absolute amplitude," *Nature Photon.*, vol. 10, pp. 267–273, Feb. 2016.

[53] E. O. Kane, "Band structure of indium antimonide," *J. Phys. Chem. Solids*, vol. 1, no. 4, pp. 249–261, 1957.

[54] A. N. Chakravarti and B. R. Nag, "Generalized Einstein relation for degenerate semiconductors having non-parabolic energy bands," *Int. J. Electron.*, vol. 37, no. 2, pp. 281–284, 1974.

[55] Y. Yang *et al.*, "Femtosecond optical polarization switching using a cadmium oxide-based perfect absorber," *Nature Photon.*, vol. 11, pp. 390–395, May 2017.

[56] M. Z. Alam, S. A. Schulz, J. Upham, I. De Leon, and R. W. Boyd, "Large optical nonlinearity of nanoantennas coupled to an epsilon-near-zero material," *Nature Photon.*, vol. 12, pp. 79–83, Jan. 2018.

[57] F. Xia, H. Wang, D. Xiao, M. Dubey, and A. Ramasubramaniam, "Two-dimensional material

nanophotonics," *Nature Photon.*, vol. 8, no. 12, pp. 899–907, Nov. 2014.
[58] Q. Guo, C. Li, B. Deng, S. Yuan, F. Guinea, and F. Xia, "Infrared nanophotonics based on graphene plasmonics," *ACS Photon.*, vol. 4, pp. 2989–2999, Aug. 2017.
[59] J. Shi *et al.*, "Thz photonics in two dimensional materials and metamaterials: Properties, devices and prospects," *J. Mater. Chem. C*, vol. 6, pp. 1291–1306, Jan. 2018.
[60] F. J. G. de Abajo, "Graphene plasmonics: Challenges and opportunities," *ACS Photon.*, vol. 1, pp. 135–152, Feb. 2014.
[61] N. K. Emani, A. V. Kildishev, V. M. Shalaev, and A. Boltasseva, "Graphene: A dynamic platform for electrical control of plasmonic resonance," *Nanophotonics*, vol. 4, no. 1, pp. 214–223, 2015.
[62] S. Xiao, X. Zhu, B.-H. Li, and N. A. Mortensen, "Graphene-plasmon polaritons: From fundamental properties to potential applications," *Frontiers Phys.*, vol. 11, Apr. 2016, Art. no. 117801.
[63] Z. Sun, A. Martinez, and F. Wang, "Optical modulators with 2D layered materials," *Nature Photon.*, vol. 10, no. 4, pp. 227–238, Apr. 2016.
[64] T. T. Tran *et al.*, "Deterministic coupling of quantum emitters in 2D materials to plasmonic nanocavity arrays," *Nano Lett.*, vol. 17, pp. 2634–2639, Mar. 2017.
[65] A. J. Giles *et al.*, "Ultralow-loss polaritons in isotopically pure boron nitride," *Nature Mater.*, vol. 17, pp. 134–139, Dec. 2017.
[66] K. Chaudhary *et al.*, "Polariton nanophotonics using phase change materials," 2019, *arXiv:1905.01277*. [Online]. Available: https://arxiv.org/abs/1905.01277
[67] L. A. Falkovsky and S. S. Pershoguba, "Optical far-infrared properties of a graphene monolayer and multilayer," *Phys. Rev. B, Condens. Matter*, vol. 76, no. 15, p. 153410, 2007.
[68] Y. Yao *et al.*, "Broad electrical tuning of graphene-loaded plasmonic antennas," *Nano Lett.*, vol. 13, no. 3, pp. 1257–1264, Feb. 2013.
[69] C.-F. Chen *et al.*, "Controlling inelastic light scattering quantum pathways in graphene," *Nature*, vol. 471, pp. 617–620, Mar. 2011.
[70] A. Vakil and N. Engheta, "Transformation optics using graphene," *Science*, vol. 332, no. 6035, pp. 1291–1294, 2011.
[71] L. Ju *et al.*, "Graphene plasmonics for tunable terahertz metamaterials," *Nature Nanotechnol.*, vol. 6, no. 10, pp. 630–634, Sep. 2011.
[72] H. Yan *et al.*, "Damping pathways of mid-infrared plasmons in graphene nanostructures," *Nature Photon.*, vol. 7, pp. 394–399, Apr. 2013.
[73] Z. Fang *et al.*, "Active tunable absorption enhancement with graphene nanodisk arrays," *Nano Lett.*, vol. 14, no. 1, pp. 299–304, 2014.
[74] S. Thongrattanasiri, F. H. L. Koppens, and F. J. G. de Abajo, "Complete optical absorption in periodically patterned graphene," *Phys. Rev. Lett.*, vol. 108, no. 4, Jan. 2012, Art. no. 047401.
[75] Z. Fang *et al.*, "Gated tunability and hybridization of localized plasmons in nanostructured graphene," *ACS Nano*, vol. 7, pp. 2388–2395, Feb. 2013.
[76] V. W. Brar, M. S. Jang, M. Sherrott, J. J. Lopez, and H. A. Atwater, "Highly confined tunable mid-infrared plasmonics in graphene nanoresonators," *Nano Lett.*, vol. 13, pp. 2541–2547, Apr. 2013.
[77] H. Yan *et al.*, "Tunable infrared plasmonic devices using graphene/insulator stacks," *Nature Nanotechnol.*, vol. 7, no. 5, pp. 330–334, May 2012.
[78] D. Rodrigo, A. Tittl, O. Limaj, F. J. G. de Abajo, V. Pruneri, and H. Altug, "Double-layer graphene for enhanced tunable infrared plasmonics," *Light-Sci. Appl.*, vol. 6, Jun. 2017, Art. no. e16277.
[79] E. Carrasco, M. Tamagnone, and J. Perruisseau-Carrier, "Tunable graphene reflective cells for THz reflectarrays and generalized law of reflection," *Appl. Phys. Lett.*, vol. 102, no. 10, 2013, Art. no. 104103.
[80] E. Carrasco, M. Tamagnone, J. R. Mosig, T. Low, and J. Perruisseau-Carrier, "Gate-controlled mid-infrared light bending with aperiodic graphene nanoribbons array," *Nanotechnology*, vol. 26, no. 13, 2015, Art. no. 134002.
[81] T. Yatooshi, A. Ishikawa, and K. Tsuruta, "Terahertz wavefront control by tunable metasurface made of graphene ribbons," *Appl. Phys. Lett.*, vol. 107, no. 5, 2015, Art. no. 053105.
[82] Z. Li, K. Yao, F. Xia, S. Shen, J. Tian, and Y. Liu, "Graphene plasmonic metasurfaces to steer infrared light," *Sci. Rep.*, vol. 5, Jul. 2015, Art. no. 12423.
[83] P.-Y. Chen, J. Soric, Y. R. Padooru, H. M. Bernety, A. B. Yakovlev, and A. Alù, "Nanostructured graphene metasurface for tunable terahertz cloaking," *New J. Phys.*, vol. 15, pp. 123029-1–123029-12, Dec. 2013.
[84] S. R. Biswas *et al.*, "Tunable graphene metasurface reflectarray for cloaking, illusion and focusing," *Phys. Rev. Appl.*, vol. 9, Mar. 2018, Art. no. 034021.
[85] H. Lin *et al.*, "A 90-nm-thick graphene metamaterial for strong and extremely broadband absorption of unpolarized light," *Nature Photon.*, vol. 13, pp. 270–276, Mar. 2019.
[86] M. Freitag, T. Low, W. Zhu, H. Yan, F. Xia, and P. Avouris, "Photocurrent in graphene harnessed by tunable intrinsic plasmons," *Nature Commun.*, vol. 4, Jun. 2013, Art. no. 1951.
[87] V. W. Brar *et al.*, "Electronic modulation of infrared radiation in graphene plasmonic resonators," *Nature Commun.*, vol. 6, May 2015, Art. no. 7032.
[88] D. Rodrigo *et al.*, "Mid-infrared plasmonic biosensing with graphene," *Science*, vol. 349, no. 6244, pp. 165–168, 2015.
[89] P.-Y. Chen, M. Farhat, A. N. Askarpour, M. Tymchenko, and A. Alù, "Infrared beam-steering using acoustically modulated surface plasmons over a graphene monolayer," *J. Opt.*, vol. 16, no. 9, 2014, Art. no. 094008.
[90] Y. Dai *et al.*, "Dynamical tuning of graphene plasmonic resonances by ultraviolet illuminations," *Adv. Opt. Mater.*, vol. 6, Mar. 2018, Art. no. 1701081.
[91] F. Valmorra *et al.*, "Low-bias active control of terahertz waves by coupling large-area CVD graphene to a terahertz metamaterial," *Nano Lett.*, vol. 13, pp. 3193–3198, Jun. 2013.
[92] W. Gao *et al.*, "High-contrast terahertz wave modulation by gated graphene enhanced by extraordinary transmission through ring apertures," *Nano Lett.*, vol. 14, pp. 1242–1248, Feb. 2014.
[93] N. K. Emani, T.-F. Chung, A. V. Kildishev, V. M. Shalaev, Y. P. Chen, and A. Boltasseva, "Electrical modulation of fano resonance in plasmonic nanostructures using graphene," *Nano Lett.*, vol. 14, no. 1, pp. 78–82, 2014.
[94] N. Dabidian *et al.*, "Electrical switching of infrared light using graphene integration with plasmonic fano resonant metasurfaces," *ACS Photon.*, vol. 2, no. 2, pp. 216–227, 2015.
[95] Z. Fang, Z. Liu, Y. Wang, P. M. Ajayan, P. Nordlander, and N. J. Halas, "Graphene-antenna sandwich photodetector," *Nano Lett.*, vol. 12, no. 7, pp. 3808–3813, 2012.
[96] S.-F. Shi *et al.*, "Optimizing broadband terahertz modulation with hybrid graphene/metasurface structures," *Nano Lett.*, vol. 15, no. 1, pp. 372–377, 2015.
[97] M. M. Jadidi *et al.*, "Tunable terahertz hybrid metal–graphene plasmons," *Nano Lett.*, vol. 15, pp. 7099–7104, Sep. 2015.
[98] Y. Yao *et al.*, "Wide wavelength tuning of optical antennas on graphene with nanosecond response time," *Nano Lett.*, vol. 14, no. 1, pp. 214–219, Dec. 2013.
[99] Y. Yao *et al.*, "Electrically tunable metasurface perfect absorbers for ultrathin mid-infrared optical modulators," *Nano Lett.*, vol. 14, pp. 6526–6532, Oct. 2014.
[100] P. Q. Liu *et al.*, "Highly tunable hybrid metamaterials employing split-ring resonators strongly coupled to graphene surface plasmons," *Nature Commun.*, vol. 6, Nov. 2015, Art. no. 8969.
[101] S. Kim, M. S. Jang, V. W. Brar, Y. Tolstova, K. W. Mauser, and H. A. Atwater, "Electronically tunable extraordinary optical transmission in graphene plasmonic ribbons coupled to subwavelength metallic slit arrays," *Nature Commun.*, vol. 7, Aug. 2016, Art. no. 12323.
[102] S. Kim, M. S. Jang, V. W. Brar, K. W. Mauser, and H. A. Atwater, "Electronically tunable perfect absorption in graphene," *Nano Lett.*, vol. 18, no. 2, pp. 971–979, 2018.
[103] S. H. Lee *et al.*, "Switching terahertz waves with gate-controlled active graphene metamaterials," *Nature Mater.*, vol. 11, pp. 936–941, Sep. 2012.
[104] N. Dabidian *et al.*, "Experimental demonstration of phase modulation and motion sensing using graphene-integrated metasurfaces," *Nano Lett.*, vol. 16, no. 6, pp. 3607–3615, May 2016.
[105] C. Qu *et al.*, "Tailor the functionalities of metasurfaces based on a complete phase diagram," *Phys. Rev. Lett.*, vol. 115, Dec. 2015, Art. no. 235503.
[106] Z. Miao *et al.*, "Widely tunable terahertz phase modulation with gate-controlled graphene metasurfaces," *Phys. Rev. X*, vol. 5, Nov. 2015, Art. no. 041027.
[107] M. C. Sherrott *et al.*, "Experimental demonstration of $>230^\circ$ phase modulation in gate-tunable graphene–gold reconfigurable mid-infrared metasurfaces," *Nano Lett.*, vol. 17, pp. 3027–3034, Apr. 2017.
[108] O. Balci *et al.*, "Electrically switchable metadevices via graphene," *Sci. Adv.*, vol. 4, Jan. 2018, Art. no. eaao1749.
[109] T.-T. Kim *et al.*, "Electrically tunable slow light using graphene metamaterials," *ACS Photon.*, vol. 5, pp. 1800–1807, Mar. 2018.
[110] T. T. Kim *et al.*, "Electrical access to critical coupling of circularly polarized waves in graphene chiral metamaterials," *Sci. Adv.*, vol. 3, Sep. 2017, Art. no. e1701377.
[111] Z. Huang *et al.*, "Graphene–metal hybrid metamaterials for strong and tunable circular dichroism generation," *Opt. Lett.*, vol. 43, no. 11, pp. 2636–2639, 2018.
[112] B. Zeng *et al.*, "Hybrid graphene metasurfaces for high-speed mid-infrared light modulation and single-pixel imaging," *Light-Sci. Appl.*, vol. 7, Aug. 2018, Art. no. 51.
[113] C. Wang *et al.*, "Dynamically tunable deep subwavelength high-order anomalous reflection using graphene metasurfaces," *Adv. Opt. Mater.*, vol. 6, no. 3, Feb. 2018, Art. no. 1701047.
[114] W. Ma, Z. Huang, X. Bai, P. Zhan, and Y. Liu, "Dual-band light focusing using stacked graphene metasurfaces," *ACS Photon.*, vol. 4, no. 7, pp. 1770–1775, 2017.
[115] S. Arezoomandan *et al.*, "Tunable terahertz metamaterials employing layered 2-D materials beyond graphene," *IEEE J. Sel. Topics Quantum Electron.*, vol. 23, no. 1, Jan./Feb. 2017, Art. no. 8500307.
[116] P. Gopalan, A. Chanana, S. Krishnamoorthy, A. Nahata, M. A. Scarpulla, and B. Sensale-Rodriguez, "Ultrafast THz modulators with WSe_2 thin films [invited]," *Opt. Mater. Exp.*, vol. 9, no. 2, pp. 826–836, 2019.
[117] F. Xiong, J. Zhang, Z. Zhu, X. Yuan, and S. Qin, "Strong anisotropic perfect absorption in monolayer black phosphorous and its application as tunable polarizer," *J. Opt.*, vol. 19, no. 7, 2017, Art. no. 075002.
[118] L. Han, L. Wang, H. Xing, and X. Chen, "Active tuning of midinfrared surface plasmon resonance and its hybridization in black phosphorus sheet array," *ACS Photon.*, vol. 5, no. 9, pp. 3828–3837, 2018.
[119] S. Xiao *et al.*, "Tunable anisotropic absorption in hyperbolic metamaterials based on black phosphorous/dielectric multilayer structures," *J. Lightw. Technol.*, to be published.
[120] K. F. Mak, C. Lee, J. Hone, J. Shan, and T. F. Heinz, "Atomically thin MoS_2: A new direct-gap semiconductor," *Phys. Rev. Lett.*, vol. 105, Sep. 2010, Art. no. 136805.
[121] P. Tonndorf *et al.*, "Photoluminescence emission and Raman response of monolayer MoS_2, $MoSe_2$,

and WSe_2," *Opt. Express*, vol. 21, no. 4, pp. 4908–4916, 2013.
[122] H. Chen *et al.*, "Manipulation of photoluminescence of two-dimensional $MoSe_2$ by gold nanoantennas," *Sci. Rep.*, vol. 6, Feb. 2016, Art. no. 22296.
[123] H. Chen, M. Liu, L. Xu, and D. N. Neshev, "Valley-selective directional emission from a transition-metal dichalcogenide monolayer mediated by a plasmonic nanoantenna," *Beilstein J. Nanotechnol.*, vol. 9, pp. 780–788, Mar. 2018.
[124] G. M. Akselrod *et al.*, "Leveraging nanocavity harmonics for control of optical processes in 2D semiconductors," *Nano Lett.*, vol. 15, pp. 3578–3584, Apr. 2015.
[125] B. Lee *et al.*, "Fano resonance and spectrally modified photoluminescence enhancement in monolayer MoS_2 integrated with plasmonic nanoantenna array," *Nano Lett.*, vol. 15, no. 5, pp. 3646–3653, 2015.
[126] Z. Wang *et al.*, "Giant photoluminescence enhancement in tungsten-diselenide–gold plasmonic hybrid structures," *Nature Commun.*, vol. 7, May 2016, Art. no. 11283.
[127] H. Zeng, J. Dai, W. Yao, D. Xiao, and X. Cui, "Valley polarization in MoS_2 monolayers by optical pumping," *Nature Nanotechnol.*, vol. 7, pp. 490–493, Jun. 2012.
[128] K. F. Mak, K. He, J. Shan, and T. F. Heinz, "Control of valley polarization in monolayer MoS_2 by optical helicity," *Nature Nanotechnol.*, vol. 7, pp. 494–498, Jun. 2012.
[129] Y. Ye *et al.*, "Electrical generation and control of the valley carriers in a monolayer transition metal dichalcogenide," *Nature Nanotechnol.*, vol. 11, pp. 597–602, Apr. 2016.
[130] Y. J. Chen, J. D. Cain, T. K. Stanev, V. P. Dravid, and N. P. Stern, "Valley-polarized exciton–polaritons in a monolayer semiconductor," *Nature Photon.*, vol. 11, pp. 431–435, Jun. 2017.
[131] Z. Sun *et al.*, "Optical control of room-temperature valley polaritons," *Nature Photon.*, vol. 11, pp. 491–496, Jul. 2017.
[132] Z. Ye *et al.*, "Probing excitonic dark states in single-layer tungsten disulphide," *Nature*, vol. 513, pp. 214–218, Sep. 2014.
[133] Y. Zhou *et al.*, "Probing dark excitons in atomically thin semiconductors via near-field coupling to surface plasmon polaritons," *Nature Nanotechnol.*, vol. 12, pp. 856–860, Jun. 2017.
[134] T. K. Fryett, K. L. Seyler, J. Zheng, C.-H. Liu, X. Xu, and A. Majumdar, "Silicon photonic crystal cavity enhanced second-harmonic generation from monolayer WSe_2," *2d Mater.*, vol. 4, no. 1, 2017, Art. no. 015031.
[135] F. Yi *et al.*, "Optomechanical enhancement of doubly resonant 2D optical nonlinearity," *Nano Lett.*, vol. 16, pp. 1631–1636, Feb. 2016.
[136] Z. Wang *et al.*, "Selectively plasmon-enhanced second-harmonic generation from monolayer tungsten diselenide on flexible substrates," *ACS Nano*, vol. 12, pp. 1859–1867, Jan. 2018.
[137] G. Hu *et al.*, "Coherent steering of nonlinear chiral valley photons with a synthetic Au–WS_2 metasurface," *Nature Photon.*, to be published. doi: 10.1038/s41566-019-0399-1.
[138] Z. Yang and S. Ramanathan, "Breakthroughs in photonics 2014: Phase change materials for photonics," *IEEE Photon. J.*, vol. 7, no. 3, Jun. 2015, Art. no. 0700305.
[139] H. W. Verleur, A. S. Barker, and C. N. Berglund, "Optical properties of VO_2 between 0.25 and 5 eV," *Phys. Rev.*, vol. 172, pp. 788–798, Aug. 1968.
[140] A. Cavalleri *et al.*, "Femtosecond structural dynamics in VO_2 during an ultrafast solid-solid phase transition," *Phys. Rev. Lett.*, vol. 87, Nov. 2001, Art. no. 237401.
[141] C. Kübler *et al.*, "Coherent structural dynamics and electronic correlations during an ultrafast insulator-to-metal phase transition in VO_2," *Phys. Rev. Lett.*, vol. 99, Sep. 2007, Art. no. 116401.
[142] D. J. Hilton *et al.*, "Enhanced photosusceptibility near T_c for the light-induced insulator-to-metal phase transition in vanadium dioxide," *Phys. Rev. Lett.*, vol. 99, Nov. 2007, Art. no. 226401.
[143] C. Chen, R. Wang, L. Shang, and C. Guo, "Gate-field-induced phase transitions in VO_2: Monoclinic metal phase separation and switchable infrared reflections," *Appl. Phys. Lett.*, vol. 93, Oct. 2008, Art. no. 171101.
[144] D. Loke *et al.*, "Breaking the speed limits of phase-change memory," *Science*, vol. 336, no. 6088, pp. 1566–1569, 2012.
[145] J. Jeong, N. Aetukuri, T. Graf, T. D. Schladt, M. G. Samant, and S. S. Parkin, "Suppression of metal-insulator transition in VO_2 by electric field–induced oxygen vacancy formation," *Science*, vol. 339, pp. 1402–1405, Mar. 2013.
[146] R. Lopez, T. E. Haynes, L. A. Boatner, L. C. Feldman, and R. F. Haglund, Jr., "Size effects in the structural phase transition of VO_2 nanoparticles," *Phys. Rev. B, Condens. Matter*, vol. 65, Jun. 2002, Art. no. 224113.
[147] Z. Chen, Y. Gao, L. Kang, C. Cao, S. Chen, and H. Luo, "Fine crystalline VO_2 nanoparticles: Synthesis, abnormal phase transition temperatures and excellent optical properties of a derived VO_2 nanocomposite foil," *J. Mater. Chem. A*, vol. 2, no. 8, pp. 2718–2727, 2014.
[148] K. Appavoo *et al.*, "Role of defects in the phase transition of VO_2 nanoparticles probed by plasmon resonance spectroscopy," *Nano Lett.*, vol. 12, pp. 780–786, Jan. 2012.
[149] J. Wei, H. Ji, W. Guo, A. H. Nevidomskyy, and D. Natelson, "Hydrogen stabilization of metallic vanadium dioxide in single-crystal nanobeams," *Nature Nanotechnol.*, vol. 7, pp. 357–362, May 2012.
[150] Y. Li, S. Ji, Y. Gao, H. Luo, and M. Kanehira, "Core-shell VO_2 TiO_2 nanorods that combine thermochromic and photocatalytic properties for application as energy-saving smart coatings," *Sci. Rep.*, vol. 3, Apr. 2013, Art. no. 1370.
[151] M. A. Kats *et al.*, "Ultra-thin perfect absorber employing a tunable phase change material," *Appl. Phys. Lett.*, vol. 101, Sep. 2012, Art. no. 221101.
[152] S. Cueff *et al.*, "Dynamic control of light emission faster than the lifetime limit using VO_2 phase-change," *Nature Commun.*, vol. 6, Oct. 2015, Art. no. 8636.
[153] J. Y. Suh, E. U. Donev, D. W. Ferrara, K. A. Tetz, L. C. Feldman, and R. F. Haglund, Jr., "Modulation of the gold particle–plasmon resonance by the metal–semiconductor transition of vanadium dioxide," *J. Opt. Pure Appl. Opt.*, vol. 10, no. 5, 2008, Art. no. 055202.
[154] T. Driscoll *et al.*, "Dynamic tuning of an infrared hybrid-metamaterial resonance using vanadium dioxide," *Appl. Phys. Lett.*, vol. 93, Jun. 2008, Art. no. 024101.
[155] M. A. Kats *et al.*, "Thermal tuning of mid-infrared plasmonic antenna arrays using a phase change material," *Opt. Lett.*, vol. 38, no. 3, pp. 368–370, 2013.
[156] D. J. Shelton, K. R. Coffey, and G. D. Boreman, "Experimental demonstration of tunable phase in a thermochromic infrared-reflectarray metamaterial," *Opt. Express*, vol. 18, no. 2, pp. 1330–1335, 2010.
[157] M. Seo *et al.*, "Active terahertz nanoantennas based on VO_2 phase transition," *Nano Lett.*, vol. 10, pp. 2064–2068, May 2010.
[158] Q.-Y. Wen, H.-W. Zhang, Q.-H. Yang, Y.-S. Xie, K. Chen, and Y.-L. Liu, "Terahertz metamaterials with VO_2 cut-wires for thermal tunability," *Appl. Phys. Lett.*, vol. 97, Jun. 2010, Art. no. 021111.
[159] T. Driscoll *et al.*, "Memory metamaterials," *Science*, vol. 325, pp. 1518–1521, Sep. 2009.
[160] K. Appavoo and R. F. Haglund, "Detecting nanoscale size dependence in VO_2 phase transition using a split-ring resonator metamaterial," *Nano Lett.*, vol. 11, pp. 1025–1031, Feb. 2011.
[161] M. Liu *et al.*, "Terahertz-field-induced insulator-to-metal transition in vanadium dioxide metamaterial," *Nature*, vol. 487, pp. 345–348, Jul. 2012.
[162] G. Xu, C.-M. Huang, M. Tazawa, P. Jin, D.-M. Chen, and L. Miao, "Electron injection assisted phase transition in a nano-au-VO_2 junction," *Appl. Phys. Lett.*, vol. 93, Jul. 2008, Art. no. 061911.
[163] M. Hada *et al.*, "Hot electron injection driven phase transitions," *Phys. Rev. B, Condens. Matter*, vol. 86, Oct. 2012, Art. no. 134101.
[164] K. Appavoo *et al.*, "Ultrafast phase transition via catastrophic phonon collapse driven by plasmonic hot-electron injection," *Nano Lett.*, vol. 14, pp. 1127–1133, Jan. 2014.
[165] D. W. Ferrara, E. R. MacQuarrie, J. Nag, A. B. Kaye, and R. F. Haglund, Jr., "Plasmon-enhanced low-intensity laser switching of gold:: Vanadium dioxide nanocomposites," *Appl. Phys. Lett.*, vol. 98, May 2011, Art. no. 241112.
[166] D. W. Ferrara, J. Nag, E. R. MacQuarrie, A. B. Kaye, and R. F. Haglund, "Plasmonic probe of the semiconductor to metal phase transition in vanadium dioxide," *Nano Lett.*, vol. 13, pp. 4169–4175, Aug. 2013.
[167] D. Y. Lei, K. Appavoo, F. Ligmajer, Y. Sonnefraud, R. F. Haglund, and S. A. Maier, "Optically-triggered nanoscale memory effect in a hybrid plasmonic-phase changing nanostructure," *ACS Photon.*, vol. 2, pp. 1306–1313, Aug. 2015.
[168] Y.-G. Jeong *et al.*, "A vanadium dioxide metamaterial disengaged from insulator-to-metal transition," *Nano Lett.*, vol. 15, pp. 6318–6323, Sep. 2015.
[169] Z. J. Thompson *et al.*, "Terahertz-triggered phase transition and hysteresis narrowing in a nanoantenna patterned vanadium dioxide film," *Nano Lett.*, vol. 15, pp. 5893–5898, Aug. 2015.
[170] O. L. Muskens *et al.*, "Antenna-assisted picosecond control of nanoscale phase transition in vanadium dioxide," *Light-Sci. Appl.*, vol. 5, Oct. 2016, Art. no. e16173.
[171] L. Liu, L. Kang, T. S. Mayer, and D. H. Werner, "Hybrid metamaterials for electrically triggered multifunctional control," *Nature Commun.*, vol. 7, Oct. 2016, Art. no. 13236.
[172] J. He *et al.*, "Terahertz tunable metasurface lens based on vanadium dioxide phase transition," *Plasmonics*, vol. 11, pp. 1285–1290, Oct. 2016.
[173] M. R. M. Hashemi, S.-H. Yang, T. Wang, N. Sepúlveda, and M. Jarrahi, "Electronically-controlled beam-steering through vanadium dioxide metasurfaces," *Sci. Rep.*, vol. 6, Oct. 2016, Art. no. 35439.
[174] M. Kim, J. Jeong, J. K. S. Poon, and G. V. Eleftheriades, "Vanadium-dioxide-assisted digital optical metasurfaces for dynamic wavefront engineering," *J. Opt. Soc. Amer. B, Opt. Phys.*, vol. 33, no. 5, pp. 980–988, Apr. 2016.
[175] J. Rensberg *et al.*, "Active optical metasurfaces based on defect-engineered phase-transition materials," *Nano Lett.*, vol. 16, no. 2, pp. 1050–1055, 2016.
[176] Z.-Y. Jia *et al.*, "Dynamically switching the polarization state of light based on the phase transition of vanadium dioxide," *Phys. Rev. Appl.*, vol. 9, Mar. 2018, Art. no. 034009.
[177] K. Dong *et al.*, "A lithography-free and field-programmable photonic metacanvas," *Adv. Mater.*, vol. 30, no. 5, 2018, Art. no. 1703878.
[178] F.-Z. Shu *et al.*, "Dynamic plasmonic color generation based on phase transition of vanadium dioxide," *Adv. Opt. Mater.*, vol. 6, no. 7, 2018, Art. no. 1700939.
[179] T. G. Follan *et al.*, "Reconfigurable infrared hyperbolic metasurfaces using phase change materials," *Nature Commun.*, vol. 9, Oct. 2018, Art. no. 4371.
[180] Z. Zhu, P. G. Evans, R. F. Haglund, and J. G. Valentine, "Dynamically reconfigurable metadevice employing nanostructured phase-change materials," *Nano Lett.*, vol. 17, pp. 4881–4885, Jul. 2017.
[181] M. Wuttig, H. Bhaskaran, and T. Taubner, "Phase-change materials for non-volatile photonic applications," *Nature Photon.*, vol. 11, pp. 465–476, Aug. 2017.

[182] N. Raeis-Hosseini and J. Rho, "Metasurfaces based on phase-change material as a reconfigurable platform for multifunctional devices," *Materials*, vol. 10, no. 9, p. 1046, 2017.

[183] A.-K. U. Michel, P. Zalden, D. N. Chigrin, M. Wuttig, A. M. Lindenberg, and T. Taubner, "Reversible optical switching of infrared antenna resonances with ultrathin phase-change layers using femtosecond laser pulses," *ACS Photon.*, vol. 1, pp. 833–839, Aug. 2014.

[184] A. Ahmadivand, B. Gerislioglu, R. Sinha, M. Karabiyik, and N. Pala, "Optical switching using transition from dipolar to charge transfer plasmon modes in $Ge_2Sb_2Te_5$ bridged metallodielectric dimers," *Sci. Rep.*, vol. 7, Feb. 2017, Art. no. 42807.

[185] B. Gholipour, J. Zhang, K. F. MacDonald, D. W. Hewak, and N. I. Zheludev, "An all-optical, non-volatile, bidirectional, phase-change meta-switch," *Adv. Mater.*, vol. 25, pp. 3050–3054, Jun. 2013.

[186] A. Tittl *et al.*, "A switchable mid-infrared plasmonic perfect absorber with multispectral thermal imaging capability," *Adv. Mater.*, vol. 27, no. 31, pp. 4597–4603, 2015.

[187] X. Yin *et al.*, "Active chiral plasmonics," *Nano Lett.*, vol. 15, no. 7, pp. 4255–4260, 2015.

[188] X. Yin *et al.*, "Beam switching and bifocal zoom lensing using active plasmonic metasurfaces," *Light-Sci. Appl.*, vol. 6, Jul. 2017, Art. no. e17016.

[189] A. Karvounis, B. Gholipour, K. F. MacDonald, and N. I. Zheludev, "All-dielectric phase-change reconfigurable metasurface," *Appl. Phys. Lett.*, vol. 109, Jul. 2016, Art. no. 051103.

[190] J. Tian *et al.*, "Active control of anapole states by structuring the phase-change alloy $Ge_2Sb_2Te_5$," *Nature Commun.*, vol. 10, Jan. 2019, Art. no. 396.

[191] C. H. Chu *et al.*, "Active dielectric metasurface based on phase-change medium," *Laser Photon. Rev.*, vol. 10, pp. 986–994, Nov. 2016.

[192] B. Gholipour, A. Karvounis, J. Yin, C. Soci, K. F. MacDonald, and N. I. Zheludev, "Phase-change-driven dielectric-plasmonic transitions in chalcogenide metasurfaces," *NPG Asia Mater.*, vol. 10, pp. 533–539, Jun. 2018.

[193] P. Hosseini, C. D. Wright, and H. Bhaskaran, "An optoelectronic framework enabled by low-dimensional phase-change films," *Nature*, vol. 511, pp. 206–211, Jul. 2014.

[194] F. F. Schlich, P. Zalden, A. M. Lindenberg, and R. Spolenak, "Color switching with enhanced optical contrast in ultrathin phase-change materials and semiconductors induced by femtosecond laser pulses," *ACS Photon.*, vol. 2, no. 2, pp. 178–182, 2015.

[195] S.-Y. Lee *et al.*, "Holographic image generation with a thin-film resonance caused by chalcogenide phase-change material," *Sci. Rep.*, vol. 7, Jan. 2017, Art. no. 41152.

[196] Q. Wang *et al.*, "Optically reconfigurable metasurfaces and photonic devices based on phase change materials," *Nature Photon.*, vol. 10, pp. 60–65, Dec. 2016.

[197] J. Sautter *et al.*, "Active tuning of all-dielectric metasurfaces," *ACS Nano*, vol. 9, no. 4, pp. 4308–4315, 2015.

[198] A. Komar *et al.*, "Electrically tunable all-dielectric optical metasurfaces based on liquid crystals," *Appl. Phys. Lett.*, vol. 110, Jan. 2017, Art. no. 071109.

[199] B. F. Soares, F. Jonsson, and N. I. Zheludev, "All-optical phase-change memory in a single gallium nanoparticle," *Phys. Rev. Lett.*, vol. 98, May 2007, Art. no. 153905.

[200] T. Lewi, H. A. Evans, N. A. Butakov, and J. A. Schuller, "Ultrawide thermo-optic tuning of PbTe meta-atoms," *Nano Lett.*, vol. 17, pp. 3940–3945, May 2017.

[201] P. P. Iyer, M. Pendharkar, and J. A. Schuller, "Electrically reconfigurable metasurfaces using heterojunction resonators," *Adv. Opt. Mater.*, vol. 4, no. 10, pp. 1582–1588, 2016.

[202] Y. Nagasaki, M. Suzuki, I. Hotta, and J. Takahara, "Control of Si-based all-dielectric printing color through oxidation," *ACS Photon.*, vol. 5, pp. 1460–1466, Jan. 2018.

[203] S. Sun *et al.*, "Real-time tunable colors from microfluidic reconfigurable all-dielectric metasurfaces," *ACS Nano*, vol. 12, pp. 2151–2159, Feb. 2018.

[204] B. Yang, W. Liu, Z. Li, H. Cheng, S. Chen, and J. Tian, "Polarization-sensitive structural colors with hue-and-saturation tuning based on all-dielectric nanopixels," *Adv. Opt. Mater.*, vol. 6, no. 4, 2018, Art. no. 1701009.

[205] Y. Gao *et al.*, "Lead halide perovskite nanostructures for dynamic color display," *ACS Nano*, vol. 12, pp. 8847–8854, Aug. 2018.

[206] A. Arbabi, Y. Horie, M. Bagheri, and A. Faraon, "Dielectric metasurfaces for complete control of phase and polarization with subwavelength spatial resolution and high transmission," *Nature Nanotechnol.*, vol. 10, no. 11, pp. 937–943, 2015.

[207] S. Wang *et al.*, "A broadband achromatic metalens in the visible," *Nature Nanotechnol.*, vol. 13, pp. 227–232, Jan. 2018.

[208] D. Lin, P. Fan, E. Hasman, and M. L. Brongersma, "Dielectric gradient metasurface optical elements," *Science*, vol. 345, no. 6194, pp. 298–302, 2014.

[209] R. C. Devlin *et al.*, "Spin-to-orbital angular momentum conversion in dielectric metasurfaces," *Opt. Express*, vol. 25, no. 1, pp. 377–393, 2017.

[210] Y.-W. Huang *et al.*, "Versatile total angular momentum generation using cascaded J-plates," *Opt. Express*, vol. 27, no. 5, pp. 7469–7484, 2019.

[211] B. H. Chen *et al.*, "GaN metalens for pixel-level full-color routing at visible light," *Nano Lett.*, vol. 17, no. 10, pp. 6345–6352, 2017.

[212] R. J. Lin *et al.*, "Achromatic metalens array for full-colour light-field imaging," *Nature Nanotechnol.*, vol. 14, pp. 227–231, Jan. 2019.

[213] E. Arbabi, A. Arbabi, S. M. Kamali, Y. Horie, M. Faraji-Dana, and A. Faraon, "MEMS-tunable dielectric metasurface lens," *Nature Commun.*, vol. 9, Feb. 2018, Art. no. 812.

[214] A. She, S. Zhang, S. Shian, D. R. Clarke, and F. Capasso, "Adaptive metalenses with simultaneous electrical control of focal length, astigmatism, and shift," *Sci. Adv.*, vol. 4, Feb. 2018, Art. no. eaap9957.

[215] A. L. Holsteen, S. Raza, P. Y. Fan, P. G. Kik, and M. L. Brongersma, "Purcell effect for active tuning of light scattering from semiconductor optical antennas," *Science*, vol. 358, pp. 1407–1410, Dec. 2017.

[216] M. R. Shcherbakov *et al.*, "Ultrafast all-optical switching with magnetic resonances in nonlinear dielectric nanostructures," *Nano Lett.*, vol. 15, pp. 6985–6990, Sep. 2015.

[217] G. D. Valle *et al.*, "Nonlinear anisotropic dielectric metasurfaces for ultrafast nanophotonics," *ACS Photon.*, vol. 4, pp. 2129–2136, Aug. 2017.

[218] M. R. Shcherbakov *et al.*, "Ultrafast all-optical tuning of direct-gap semiconductor metasurfaces," *Nature Commun.*, vol. 8, May 2017, Art. no. 17.

[219] S. Liu *et al.*, "An all-dielectric metasurface as a broadband optical frequency mixer," *Nature Commun.*, vol. 9, Jun. 2018, Art. no. 2507.

[220] D. Schurig *et al.*, "Metamaterial electromagnetic cloak at microwave frequencies," *Science*, vol. 314, no. 5801, pp. 977–980, Oct. 2006.

[221] C. Pfeiffer and A. Grbic, "Metamaterial Huygens' surfaces: Tailoring wave fronts with reflectionless sheets," *Phys. Rev. Lett.*, vol. 110, no. 19, p. 197401, May 2013.

[222] X. Wu *et al.*, "Active microwave absorber with the dual-ability of dividable modulation in absorbing intensity and frequency," *AIP Adv.*, vol. 3, no. 2, p. 022114, Feb. 2013.

[223] C. Huang *et al.*, "Reconfigurable metasurface cloak for dynamical electromagnetic illusions," *ACS Photon.*, vol. 5, no. 5, pp. 1718–1725, 2018.

[224] H.-X. Xu *et al.*, "Dynamical control on helicity of electromagnetic waves by tunable metasurfaces," *Sci. Rep.*, vol. 6, Jun. 2016, Art. no. 27503.

[225] X. Gao, W. L. Yang, H. F. Ma, Q. Cheng, X. H. Yu, and T. J. Cui, "A reconfigurable broadband polarization converter based on an active metasurface," *IEEE Trans. Antennas Propag.*, vol. 66, no. 11, pp. 6086–6095, Nov. 2018.

[226] Z. Tao, X. Wan, B. C. Pan, and T. J. Cui, "Reconfigurable conversions of reflection, transmission, and polarization states using active metasurface," *Appl. Phys. Lett.*, vol. 110, Mar. 2017, Art. no. 121901.

[227] H.-X. Xu *et al.*, "Tunable microwave metasurfaces for high-performance operations: Dispersion compensation and dynamical switch," *Sci. Rep.*, vol. 6, Nov. 2016, Art. no. 38255.

[228] H.-X. Xu *et al.*, "Aberration-free and functionality-switchable meta-lenses based on tunable metasurfaces," *Appl. Phys. Lett.*, vol. 109, Oct. 2016, Art. no. 193506.

[229] K. Chen *et al.*, "A reconfigurable active huygens' metalens," *Adv. Mater.*, vol. 29, May 2017, Art. no. 1606422.

[230] T. J. Cui, M. Q. Qi, X. Wan, J. Zhao, and Q. Cheng, "Coding metamaterials, digital metamaterials and programmable metamaterials," *Light-Sci. Appl.*, vol. 3, Oct. 2014, Art. no. e218.

[231] Y. B. Li *et al.*, "Transmission-type 2-bit programmable metasurface for single-sensor and single-frequency microwave imaging," *Sci. Rep.*, vol. 6, Mar. 2016, Art. no. 23731.

[232] L. Li *et al.*, "Electromagnetic reprogrammable coding-metasurface holograms," *Nature Commun.*, vol. 8, Aug. 2017, Art. no. 197.

[233] X. G. Zhang *et al.*, "Light-controllable digital coding metasurfaces," *Adv. Sci.*, vol. 5, Nov. 2018, Art. no. 1801028.

[234] X. G. Zhang, W. X. Jiang, and T. J. Cui, "Frequency-dependent transmission-type digital coding metasurface controlled by light intensity," *Appl. Phys. Lett.*, vol. 113, Aug. 2018, Art. no. 091601.

[235] J. Zhao *et al.*, "Programmable time-domain digital coding metasurface for nonlinear harmonic manipulation and new wireless communication systems," *Nat. Sci. Rev.*, 2018, Art. no. nwy135.

[236] L. Zhang *et al.*, "Space-time-coding digital metasurfaces," *Nature Commun.*, vol. 9, no. 1, p. 4334, 2018.

[237] L. Wang *et al.*, "Slow cooling and efficient extraction of c-exciton hot carriers in MoS_2 monolayer," *Nature Commun.*, vol. 8, Jan. 2017, Art. no. 13906.

[238] J. P. B. Mueller, N. A. Rubin, R. C. Devlin, B. Groever, and F. Capasso, "Metasurface polarization optics: Independent phase control of arbitrary orthogonal states of polarization," *Phys. Rev. Lett.*, vol. 118, no. 11, p. 113901, 2017.

[239] W. T. Chen *et al.*, "A broadband achromatic metalens for focusing and imaging in the visible," *Nature Nanotechnol.*, vol. 13, pp. 220–226, Jan. 2018.

[240] S. Wang *et al.*, "Broadband achromatic optical metasurface devices," *Nature Commun.*, vol. 8, Aug. 2017, Art. no. 187.

[241] D. Sell, J. Yang, S. Doshay, R. Yang, and J. A. Fan, "Large-angle, multifunctional metagratings based on freeform multimode geometries," *Nano Lett.*, vol. 17, pp. 3752–3757, May 2017.

[242] Z. Lin, B. Groever, F. Capasso, A. W. Rodriguez, and M. Lončar, "Topology-optimized multilayered metaoptics," *Phys. Rev. Appl.*, vol. 9, Apr. 2018, Art. no. 044030.

[243] R. Pestourie, C. Pérez-Arancibia, Z. Lin, W. Shin, F. Capasso, and S. G. Johnson, "Inverse design of large-area metasurfaces," *Opt. Express*, vol. 26, no. 26, pp. 33732–33747, 2018.

ABOUT THE AUTHORS

Yao-Wei Huang received the B.S. degree in optics and photonics from the National Central University, Taoyuan, Taiwan, in 2010, and the M.S. and Ph.D. degrees with Dean's Awards in applied physics from the National Taiwan University, Taipei, Taiwan, in 2012 and 2015, respectively.

He has been a Research Fellow with the National University of Singapore, Singapore, since 2016, and a Postdoctoral Fellow with Harvard University, Cambridge, MA, USA, since 2017. His current research interests include nanophotonics, metasurfaces, and biomedical images. His work is focused on the low-loss metasurfaces, tunable metasurfaces, and their applications.

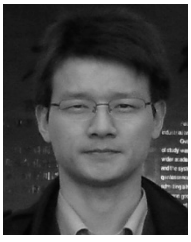

He-Xiu Xu (Senior Member, IEEE) was born in Jiujiang, China, in 1985. He received the B.S. degree in radar engineering and the Ph.D. degree in electronic science and technology from Air Force Engineering University, Xi'an, China, in 2008 and 2014, respectively.

He was a Visiting Scholar with Southeast University, Nanjing, China, from 2012 to 2014, a Postdoctoral Fellow with Fudan University, Shanghai, China, from 2015 to 2017, and a Visiting Scholar with the National University of Singapore, Singapore, from 2017 to 2018. He joined the Air Force Engineering University in 2014 and was promoted to an Associate Professor in 2016. He is currently a Guest Professor with Hengyang Normal University, Hengyang, China. He has published more than 85 peer-reviewed first-authored/coauthored journal papers, two Chinese books, and two English book chapters. He has owned 24 China patents and has given about 14 invited talks. His current research interests include passive/active metamaterials/metasurfaces and their applications to novel microwave functional devices and antennas.

Dr. Xu is a Senior Member of CIE. He received the 8th China Youth Science and Technology Innovation Award in 2013, the Best Excellent Doctoral Dissertation Award at Air Force Engineering University in 2014, the Excellent Doctoral Dissertation Award from Military, Shaanxi Province, and the Chinese Institute of Electronics (CIE), the URSI AP-RASC Young Scientist Award, the URSI EMTS Young Scientist Award in 2019, the Outstanding Scientific and Technological Worker of CIE in 2018, the Young Talent from the China Association for Science and Technology in 2017, the Young Scientist Nova from the Shaanxi Technology Committee in 2016, and several scientific and technological progress awards. He was a recipient of the Excellent Paper Award in metasurface multifunctional devices at the 23th Annual Youth Conference of CIE in 2017 and in helicity control of metasurface at the Progress in Electromagnetic Research Symposium in 2018 and a co-recipient of the Best Paper Award in bifunctional metasurfaces at the A3 Metamaterials Forum in 2017. He has been serving as an Editor for the *AEU–International Journal of Electronics and Communications* since 2014. He served as a Guest Editor for Special Issue "Metamaterial Circuits and Antennas" of the *International Journal of RF and Microwave Computer-Aided Engineering* in 2018 and an invited reviewer for more than 20 leading journals. He served as the special session chair eight times and a TPC co-chair/member more than 12 times in international conferences.

Shang Sun received the B.S. degree in optical information science and technology, the M.S. degree in optics, and the Ph.D. degree in physics and chemistry of materials from Harbin Institute of Technology, Harbin, China, in 2012, 2014, and 2018, respectively.

In 2018, he joined the group of Prof. C.-W. Qiu as a Postdoctoral Research Fellow at the National University of Singapore, Singapore. His current research interests include nanophotonics, metamaterials, and optical and reconfigurable metasurfaces.

Yunkai Wu received the B.S. degree in material chemistry from Harbin Institute of Technology, Harbin, China, in 2017. He is currently working toward the Ph.D. degree in material science at Harbin Institute of Technology at Shenzhen, Shenzhen, China.

His current research interests include microfabrication and nanofabrication and the optical design of metasurface.

Zhuo Wang received the B.S. and M.E. degrees from Sichuan University, Chengdu, China, in 2010 and 2013, respectively, and the joint Ph.D. degree from the National University of Singapore, Singapore, and Imperial College London, London, U.K., in 2017.

She is currently an Assistant Professor with the International Collaborative Laboratory of 2D Materials for Optoelectronics Science and Technology, Shenzhen University, Shenzhen, China. Her current research interests include optoelectronic devices based on 2-D materials and optical properties of plasmon-enhanced 2-D materials.

Shumin Xiao received the Ph.D. degree from the Department of Electrical Engineering and Computer Science, Purdue University, West Lafayette, IN, USA, in 2010.

After one-year postdoctoral work at Purdue University, she joined Harbin Institute of Technology as the National Thousand Youth Talents Plan Professor of China in 2011. Her current research interests include integrated optoelectronics, semiconductor devices, metamaterials, plasmonic physics and devices, nonlinear optics, and nanophotonics.

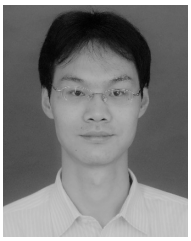

Wei Xiang Jiang (Member, IEEE) was born in Yancheng, China, in 1981. He received the Ph.D. degree in electrical engineering from Southeast University, Nanjing, China, in 2011.

He joined the State Key Laboratory of Millimeter Waves, Southeast University, in 2010, and was promoted to the post of Associate Professor in 2011 and Professor in 2015. He has published more than 70 peer-reviewed journal papers in *Advanced Materials*, the IEEE TRANSACTIONS ON ANTENNAS AND PROPAGATION, *Materials Today*, *Applied Physics Letters*, and so on. His current research interests include the theory and applications of metamaterials and metasurfaces.

Dr. Jiang's works have been selected as "Research Highlights" by *Europhysics News* journal in 2008, "Research Highlights in 2008" by the *Journal of Physics D: Applied Physics*, and "Research Highlights" by *Applied Physics Letters* in 2011. He received the First Prize of Natural Science from the Ministry of Education, China, in 2011 (Rank 2), the National Excellent Doctoral Dissertation in 2013, and the Second Prize of National Natural Science Awards, China, in 2014 and 2018 (Rank 3), and the Young Scientist Award from the International Union of Radio Science (URSI) in 2014. He has served as the Organization Committee Co-Chair of the International Workshop on Metamaterials (META'2012, Nanjing) and the TPC Co-Chair of the International Symposium on Plasmonics and Nano-photonics (iSPN2017Dalian). He is also an active reviewer of several journals, including the *New Journal of Physics*, the *Journal of Physics D: Applied Physics*, the *Journal of Optics*, and *Chinese Physics Letters*.

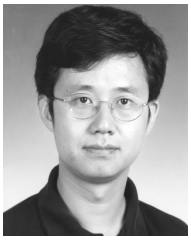

Tie Jun Cui (Fellow, IEEE) was born in Chengde, China, in 1965. He received the B.Sc., M.Sc., and Ph.D. degrees in electrical engineering from Xidian University, Xi'an, China, in 1987, 1990, and 1993, respectively.

In 1993, he joined the Department of Electromagnetic Engineering, Xidian University, and was promoted to an Associate Professor in 1993. From 1995 to 1997, he was a Research Fellow with the Institut fur Hochstfrequenztechnik und Elektronik (IHE), University of Karlsruhe, Karlsruhe, Germany. In 1997, he joined the Center for Computational Electromagnetics, Department of Electrical and Computer Engineering, University of Illinois at Urbana–Champaign, Champaign, IL, USA, first as a Postdoctoral Research Associate and then as a Research Scientist. In 2001, he was a Cheung Kong Professor with the Department of Radio Engineering, Southeast University, Nanjing, China. In 2018, he became the Chief Professor at Southeast University. He is the first author of the books: *Metamaterials: Theory, Design, and Applications* (Springer, 2009) and *Metamaterials: Beyond Crystals, Noncrystals, and Quasicrystals* (CRC Press, 2016). He has published over 400 peer-reviewed journal papers in *Science*, *Proceedings of the National Academy of Sciences (PNAS)*, *Nature Communications*, *Physical Review Letters*, *Advanced Materials*, and IEEE TRANSACTIONS, which have been cited by more than 21 400 times (H-Factor 74).

Dr. Cui received a Research Fellowship from the Alexander von Humboldt Foundation, Bonn, Germany, in 1995, the Young Scientist Award from the International Union of Radio Science (URSI) in 1999, the Cheung Kong Professor under the Cheung Kong Scholar Program by the Ministry of Education, China, in 2001, the National Science Foundation of China for Distinguished Young Scholars in 2002, the First Prize of the Natural Science Awards from the Ministry of Education, China, in 2011, the Second Prize of the National Natural Science Awards, China, in 2014, the First Prize of the Military Science and Technology Progress Awards in 2016, and the Second Prize of the National Natural Science Awards, China, in 2018. His works have been selected as one of the "Optics in 2016" by the Optics and Photonics News Magazine (OSA), "10 Breakthroughs of China Optics in 2016," "10 Breakthroughs of China Science in 2010," and "Best of 2010" in *New Journal of Physics*. According to Elsevier, he is one of the Most Cited Chinese Researchers. His work has been reported by *Nature News*, *Science*, *MIT Technology Review*, *Scientific American*, *New Scientists*, and so on. He served as the General Co-Chair of the International Workshops on Metamaterials (META 2008 and META 2012), the TPC Co-Chair of the Asian Pacific Microwave Conference (APMC 2005) and the Progress in Electromagnetic Research Symposium (PIERS 2004). He is an Active Reviewer of *Science*, *Nature Materials*, *Nature Photonics*, *Nature Physics*, *Nature Communications*, *Physical Review Letters*, *Advanced Materials*, and a series of IEEE TRANSACTIONS. He was an Associate Editor of the IEEE TRANSACTIONS ON GEOSCIENCE AND REMOTE SENSING and a Guest Editor of *Science China Information Sciences*.

Din Ping Tsai (Fellow, IEEE) received the Ph.D. degree in physics from the University of Cincinnati, Cincinnati, OH, USA, in 1990.

He has been a Distinguished Research Fellow with the Research Center for Applied Sciences, Academia Sinica, Taipei, Taiwan, since 2012. He has been a Distinguished Professor with the Department of Physics, National Taiwan University, Taipei, since 2006, and a Chair Professor with the Department of Materials Science and Engineering, National Tsing Hua University, Hsinchu, Taiwan, since 2018.

Dr. Tsai is a Fellow of the American Association for the Advancement of Science (AAAS), the Academician of Asia-Pacific Academy of Materials (APAM), the American Physical Society (APS), the Electro Magnetics Academy (EMA), the International Academy of Engineering (IAE), the Japan Society of Applied Physics (JSAP), the Optical Society of America (OSA), and the International Society of Optical Engineering (SPIE).

Cheng-Wei Qiu (Member, IEEE) received the B.Eng. degree from the University of Science and Technology of China, Hefei, China, in 2003 and the Ph.D. degree from the National University of Singapore (NUS), Singapore, in 2007.

He was a Postdoctoral Fellow with the Physics Department, Massachusetts Institute of Technology (MIT), Cambridge, MA, USA, until 2009. In 2009, he joined the NUS as an Assistant Professor and was promoted to Associate Professor with tenure in 2017. In 2018, he was promoted to Dean's Chair Professor at the Faculty of Engineering, NUS. His research is known for the structured light for beam manipulation and nanoparticle manipulation.

Dr. Qiu was a recipient of the SUMMA Graduate Fellowship in Advanced Electromagnetics in 2005, the IEEE AP-S Graduate Research Award in 2006, the URSI Young Scientist Award in 2008, the NUS Young Investigator Award in 2011, the MIT TR35@Singapore Award in 2012, the Young Scientist Award by the Singapore National Academy of Science in 2013, the Faculty Young Research Award in NUS 2013, and the Young Engineering Research Award 2018 from NUS.